# A Parabrachial to Hypothalamic Neurocircuit Mediates Defensive Behavior

Fan Wang[1,2†], Yuge Chen[1,2†], Yuxin Lin[1,2$], Xuze Wang[1,2$], Kaiyuan Li[1,2], Yong Han[1,2], Jintao Wu[1,2], Xingyi Shi[1,2], Zhenggang Zhu[1,2], Chaoying Long[1,2], Xiaojun Hu[1,3], Shumin Duan[1,2,3,4,5,6]* and Zhihua Gao[1,2,3]*

[1]Department of Neurobiology and Department of Neurosurgery of Second Affiliated Hospital, Zhejiang University School of Medicine, Hangzhou, P.R. China;

[2]Liangzhu Laboratory, Zhejiang University Medical Center, Hangzhou, P.R. China.

[3]NHC and CAMS Key Laboratory of Medical Neurobiology, MOE Frontier Science Center for Brain Science and Brain-Machine Integration, School of Brain Science and Brain Medicine, Zhejiang University, Hangzhou, P.R. China;

[4]Institute for Translational Brain Research, MOE Frontiers Center for Brain Science, Fudan University, Shanghai, P.R. China;

[5]The Institute of Brain and Cognitive Sciences, Zhejiang University City College, Hangzhou, P.R. China;

[6]Chuanqi Research and Development Center of Zhejiang University, Hangzhou, P.R. China

[†]These authors contributed equally to this work

[$] These authors contributed equally to this work

*For correspondence: duanshumin@zju.edu.cn (S.D.); zhihuagao@zju.edu.cn (Z.G.)

**Abstract**

Defensive behaviors are critical for animal's survival. The parabrachial nucleus (PBN) is critical in transmitting danger stimuli to trigger behavioral responses. Here, by viral tracing and electrophysiological recordings, we uncover that cholecystokinin (CCK) neurons in the lateral PB ($LPB^{CCK}$ neurons) are monosynaptically connected with the paraventricular nucleus (PVN) neurons. Selective photoactivation of $LPB^{CCK}$ neurons, their axon terminals within the PVN and glutamatergic neurons in the PVN, trigger defensive-like flight-to-nest behavior. Conversely, photoinhibition of $LPB^{CCK}$ neurons suppresses defensive responses. We further show that $LPB^{CCK}$ neurons provide excitatory transmission to the PVN neurons, and blocking glutamatergic transmission inhibits $LPB^{CCK}$-PVN pathway activation-induced flight behaviors. Also, chemogenetic inhibition of PVN neurons prevents photoactivation of $LPB^{CCK}$-PVN pathway-driven flight responses. These data suggest that $LPB^{CCK}$ neurons recruit downstream PVN neurons to actively engage in flight responses. Our study identifies a novel circuit from $LPB^{CCK}$ to PVN and dissects its role in defensive behaviors.

## Introduction

Living in an environment full of diverse threats, animals develop a variety of defensive behaviors for survival during evolution (Anderson & Adolphs, 2014; Blanchard et al., 2001; Crawford & Masterson, 1982; Fanselow & Bolles, 1979; LeDoux, 2012; Yilmaz & Meister, 2013). From the perspective of predator and prey interactions, defensive responses are generally divided into two categories: defensive behaviors avoiding being discovered (for example, freezing or hiding behaviors) and defensive behaviors avoiding being caught (for example, running or attacking behaviors) (Crawford & Masterson, 1982; Fanselow & Bolles, 1979; Yilmaz & Meister, 2013). Which type of defensive behavior is selected depends on many factors, such as the distance from threat and access to shelters. In general, escape is triggered when animals are faced with an imminent threat with a shelter nearby (Eilam, 2005; Perusini & Fanselow, 2015; L. Sun et al., 2020; Zhang et al., 2018).

Several brain regions, including the periaqueductal gray (PAG), amygdala and medial hypothalamic zone (MHZ), have been implicated in mediating escape behaviors (Evans et al., 2018; Shang et al., 2018; Shang et al., 2015; Silva et al., 2013; Tovote et al., 2016; Wang et al., 2015; Wang, Schuette, Nagai, et al., 2021; Wei et al., 2015). Recent studies have highlighted a role for MHZ, including the anterior hypothalamic nucleus (AHN), the dorsomedial part of ventromedial hypothalamic nucleus (VMHdm) and the dorsal pre-mammillary nucleus (PMd), in mediating escape behaviors. For example, projections from PMd to the dorsolateral periaqueductal gray region (dlPAG) and those from PVN to the anteromedial ventral thalamic region (AMV) have been

shown to control escape behaviors (Wang, Schuette, Nagai, et al., 2021). Another study showed that a subset of VMH neurons collaterally project to the AHN and PAG to promote escape and avoidance behaviors (Wang et al., 2015). In addition, PVN, an area enriched with endocrine neurons, has also been associated with escape behaviors. Optogenetic activation of Sim1$^{+}$ neurons in the PVN triggers escape behavior (Mangieri et al., 2019b). Projections from PVN to the ventral midbrain region (vMB) mediate profound defensive-like behaviors, including hiding, escape jumping, hyperlocomotion (Mangieri et al., 2019b), whereas projections from PVN to the ventral lateral septum (LSv) drive fear-related escape jumping (Xu et al., 2019). Despite a growing number of studies illustrating the importance of PVN in mediating defensive behaviors, upstream input that transmit the danger signals to PVN remains unclear.

The parabrachial nucleus located in the dorsolateral pons, serves as a relay station for sensory transmission during the aversive sensory processes (Fulwiler & Saper, 1984). PBN bears association with various sensory processes including the pain, itch, hunger, and thermoregulation to protect the body from noxious stimuli (Alhadeff et al., 2018; Campos et al., 2017; Campos et al., 2018; Carter et al., 2013; Chen et al., 2018; Geerling et al., 2016; Kobayashi & Osaka, 2003; Mu et al., 2017; Nakamura & Morrison, 2008, 2010; Uddin et al., 2018). In addition, PBN contains several subregions with diverse peptide-expressing neuronal subtypes. The external lateral nuclei of PBN (PBel), rich in calcitonin gene-related peptide (CGRP) neurons, plays an important role in affective-behavior states to limit the harm caused by potential threats, such as painful stimuli, itch-related stimuli, novel foods (Campos et al., 2018; Carter et al., 2013;

Gauriau & Bernard, 2002; Han et al., 2015; Kobayashi & Osaka, 2003). The dorsal lateral area of PB (PBdl) contains dynorphin neurons and is crucial for thermoregulation (Norris et al., 2021). The superior lateral area of PB (PBsl) contains a large number of CCK neurons, which has been linked to glucose regulation via projections to VMH (Garfield et al., 2014) and heat defense via projections to preoptic area (POA) (Yang et al., 2020). Among these peptide-expressing neurons, CGRP neurons in the LPB are implicated in defensive behavior under stressful or threatening circumstances. $LPB^{CGRP}$ neurons have been implicated in encoding alarm response by projecting to a number of limbic regions including the amygdala and bed nucleus of stria terminalis (BNST). It remains unclear whether neurons in the LPB are directly connected to the hypothalamus to mediate defensive behaviors.

CCK and CCK receptor-expressing neurons have been associated with defensive behaviors (Bertoglio et al., 2007; Chen et al., 2022; Wang, Schuette, La-Vu, et al., 2021). PVN neurons also express CCK receptors and are involved in defensive behaviours (Mangieri et al., 2019a; O'Shea & Gundlach, 1993; Xu et al., 2019), raising a possibility that upstream CCK input to the PVN may be implicated in defensive behaviours. In attempting to answer these questions, we firstly injected the Cre-dependent retrograde tracer (AAV2-Retro-DIO-EYFP) into the PVN of CCK-Cre mice and found that LPB was an important upstream area transmission to the PVN. By electrophysiological analyses, we verified the direct connections between $LPB^{CCK}$ neurons and PVN neurons. Using optogenetic tools, we showed that activation of $LPB^{CCK}$ neurons drove rapid flight-to-nest behaviors, whereas inhibition of $LPB^{CCK}$

111 neurons suppressed heat-evoked defensive behaviors, suggesting that $LPB^{CCK}$ neurons
112 were sufficient and required for defensive behaviors. Interestingly, photoactivation of
113 terminals from $LPB^{CCK}$ to PVN or activation of $PVN^{Vglut2}$ neurons alone also elicited
114 flight-to-nest behavior. Both chemogenetic inhibition of PVN neurons and
115 pharmacological blockade of glutamatergic transmission prevented axonal termianl
116 activation of $LPB^{CCK}$ within the PVN-induced flight-to-nest behavior, suggesting that
117 PVN was an important target mediating $LPB^{CCK}$-driven defensive responses. Our data
118 suggest a novel neurocircuit that mediates defensive behavior, which may shed light on
119 the mechanism of fear-related psychiatric diseases.
120

121 **Results**

122 **$CCK^+$ neurons in the LPB provides monosynaptic glutamatergic projections to the**
123 **PVN**

124 To identify the upstream CCKergic inputs to the PVN, we injected the retrograde viral
125 tracer (AAV2-Retro-DIO-EYFP, hereafter referred to as AAV2-Retro) into the PVN
126 region of a knock-in mouse line expressing Cre recombinase at the CCK Locus (CCK-
127 ires-Cre) **(Figure 1A)**. We observed abundant $EYFP^+$ neurons in the medial orbital
128 cortex (MO), cingulate cortex (CC), LPB and scattered $GFP^+$ cells in the PAG and
129 dysgranular insular cortex (DI) **(Figure 1B-C，Supplementary Fig.1).** Among these
130 nuclei, we mainly focused on the LPB, a region critical for sensory signal processing
131 (Fulwiler, C.E., and Saper, C.B.,1985; Garfield AS et al., 2014). To further verify the
132 anatomical connections between the LPB and PVN, we injected the anterograde viral

133 tracer (AAV-hSyn-FLEx-mGFP-2A-Synaptophysin-mRuby) into the LPB of CCK-Cre
134 mice **(Figure 1D)**. We found that prominent $GFP^+$ fibers and $mRuby^+$ bouton-like
135 structures, reminiscent axonal terminals, within the PVN, indicating that $LPB^{CCK}$
136 neurons directly project to the PVN **(Figure 1E-F, Supplementary Fig 2).**

137 $CCK^+$ neurons have been shown to primarily located within PBsl (Garfield et al.,
138 2014). To further visualize and characterize $LPB^{CCK}$ neurons, we crossed the CCK-ires-
139 Cre mice with the Cre-dependent tdTomato (tdT) reporter line (Ai14) and found that
140 the expression of CCK was abundantly expressed in the rostral and mid LPB **(Figure**
141 **2A-C)**. The majority of LPB neurons have been shown to be glutamatergic neurons
142 with a small population being GABAergic (Geerling et al., 2016; Kaur et al., 2013). To
143 dissect the identity of $CCK^+$ neurons in the LPB, we performed *in situ* hybridization in
144 CCK-ires-Cre::Ai14 mice using probes for *Vglut2* and *Vgat*, markers specific to
145 glutamatergic and GABAergic neurons. We found that $LPB^{CCK}$ neurons (84.0% ± 1.7%)
146 predominantly expressed *Vglut2*, with a tiny subpopulation (2.0% ± 1.2%) expressed
147 *Vgat*, suggesting that $LPB^{CCK}$ neurons were mostly glutamatergic neurons. In addition,
148 co-labeling with another neuropeptide, CGRP, in these mice revealed a slight co-
149 localization (2.2% ± 0.37%) between CCK and CGRP **(Figure 2D-G)**, suggesting a
150 separation between these two subpopulations of neurons within different areas of LPB.
151 Collectively, these data indicate that CCK neurons comprise a subpopulation of
152 glutamatergic neurons and barely overlap with CGRP neurons within the LPB.

153 Next, we used electrophysiological recording to investigate the functional
154 connections between the LPB and PVN by injecting the Cre-dependent adeno-

155 associated virus (AAV) expressing channelrhodopsin-2 virus (AAV2/9-DIO-ChR2-
156 EYFP) into the LPB of CCK-Cre mice **(Figure 2H)**. By optic stimulating the axonal
157 terminals of $LPB^{CCK}$ neurons within the PVN, we successfully recorded excitatory
158 postsynaptic currents (EPSCs), rather than inhibitory postsynaptic currents (IPSCs).
159 These EPSCs were blocked in the presence of a sodium channel antagonist TTX and
160 rescued by the potassium channel antagonist 4-AP, suggesting monosynaptic
161 connections between these neurons. Further, the EPSCs were blocked by NMDA
162 receptor antagonist AP5 **(Figure 2I)**, and AMPA receptor antagonist CNQX **(Figure**
163 **2J-K)**. These data suggest that neurons in the PVN receive monosynaptic excitatory
164 innervations from $LPB^{CCK}$ neurons.

165

166 **Photostimulation of $LPB^{CCK}$ neurons triggers defensive-like flight-to-nest**
167 **behavior**

168 Previous studies have shown that $LPB^{CCK}$ neurons participate in the regulation of
169 glucose homeostasis through SF1 neurons in the VMH (Garfield et al., 2014) and
170 thermoregulation via connections with the POA (Yang et al., 2020). It remains unclear
171 what effects direct optogenetic activation of $LPB^{CCK}$ neurons may induce. We firstly
172 tested the efficacy of ChR2-mediated activation by injecting the AAV2/9-DIO-ChR2-
173 EYFP virus into the LPB of CCK-Cre mice and carried out whole-cell recordings from
174 brain slices for viral-infected neurons. As shown in **Figure 3A**, different frequencies of
175 blue laser pulses (from 5-20 Hz) induced time-locked action potential firing in $LPB^{CCK}$
176 neurons expressing ChR2, with 20 Hz inducing maximal firing capacities, verifying the

effectiveness of optic tools.

PBN is an important relay nucleus that transmits peripheral sensations to the brain to limit harm (Campos et al., 2018). Recent studies have found that $LPB^{CGRP}$ neurons play an important role in mediating fear-related behaviors (Campos et al., 2018; Han et al., 2015). It remains unclear whether $LPB^{CCK}$ neurons also participate in fear-related behaviors. To determine whether $LPB^{CCK}$ neurons mediate fear-related behavior, we optically activated these neurons as described above **(Figure 3B-3C)**, and investigated fear-related defensive-like behaviors in mice using a flight-to-nest test experimental paradigm previously used (Zhou et al., 2019). We placed a nest in the corner to test the ability of mice to actively search for hiding. Optogenetic activation of ChR2-expressing CCK neurons induced defensive-like flight-to-nest behavior in the experimental apparatus, as mice escaped towards the nest (latency: EYFP 87.71 ± 22.38 s versus ChR2 7.571 ± 0.8123 s; speed: EYFP 184.4% ± 30.4% versus ChR2 361.7% ± 31.5%) followed by long-lasting time stay in the nest (EYFP 63.906% ± 3.645% versus ChR2 97.26% ± 2.737%) **(Figure 3D-J)**. Our data suggest that activation of $LPB^{CCK}$ neurons is sufficient to drive defensive-like flight-to-nest behavior.

**Photostimulation of $LPB^{CCK}$ neurons induces anxiety-like behavior and autonomic responses**

Since activation of $LPB^{CCK}$ neurons induced fear-related flight-to-nest behavior, and long-term fear may trigger an anxiety-like state in animals (Tovote et al., 2005; Yang et al., 2016), we next determined whether mice exhibit anxiety-like behaviors after

199 prolonged activation of $LPB^{CCK}$ neurons. We gave mice 10-min of light stimulation and
200 tested their responses in the open field and elevated plus maze 20-min later **(Figure**
201 **4A)**. We found that optogenetic stimulation of $LPB^{CCK}$ neurons expressing ChR2-
202 EYFP, but not those expressing EYFP, significantly reduced the total distance, center
203 time and center entries in the open field tests, as well as the open arm time and open
204 arm entries in the elevated plus maze tests **(Figure 4B-E)**. Our results indicate that
205 prolonged optogenetic manipulation of $LPB^{CCK}$ neurons induces anxiety-like behaviors.
206 When animals and humans face danger, the sympathetic nervous system is usually
207 activated, as characterized by increased heart rates and dilated pupil size (Dong et al.,
208 2019; Gross & Canteras, 2012; Wang et al., 2015). We found that photostimulation of
209 $LPB^{CCK}$ neurons significantly increased heart rate and enlarged pupil diameter,
210 suggesting a fast arousal state (Salay et al., 2018) **(Figure 4F-J)**. Moreover, plasma
211 levels of corticosterone were also increased upon photostimulation of $LPB^{CCK}$ neurons
212 **(Figure 4K)**, indicating a stress-related response in mice. In summary, photoactivation
213 of $LPB^{CCK}$ neurons induces accompanying changes in sympathetic nervous system and
214 stress responses in mice.
215
216 **Inhibition of $LPB^{CCK}$ neurons suppressed heat-evoked defensive behavior**
217 To examine whether $LPB^{CCK}$ neurons are required for defensive behavior, we then
218 inhibited $LPB^{CCK}$ neurons using optogenetic tools. By injecting the Cre-dependent
219 adeno-associated virus (AAV) expressing the guillardia theta anion channel
220 rhodopsins-1 (GtACR1) into the LPB of CCK-Cre mice, followed by optic stimulation,

221 we were able to effectively inhibit the firing of $LPB^{CCK}$ neurons **(Figure 5A)**.

222 Mammals are sensitive to temperature changes and develop multiple mechanisms
223 to avoid excessive high or low temperature. When confronted extreme heat or cold,
224 animals would turn to an area with comfortable temperature. Since $LPB^{CCK}$ neurons
225 have been recently shown to be implicated in thermosensation (Yang et al., 2020), we
226 speculated that they may mediated heat defense. To determine whether $LPB^{CCK}$ neurons
227 might be involved in heat defense, we designed an apparatus, which containing two
228 zones of different temperatures, 25 degree, the comfortable zone at room temperature,
229 and 43 degree, the uncomfortable zone at a higher temperature which induces
230 uncomfortable feeling but not pain (Wang, Schuette, Nagai, et al., 2021). To test
231 whether inhibition of $LPB^{CCK}$ neurons suppressed heat-evoked defensive behaviors, we
232 bilaterally injected Cre-dependent virus (AAV-CAG-DIO-GtACR1-EYFP or AAV-
233 CAG-DIO-EYFP) into LPB and positioned optical fibers above the LPB of CCK-Cre
234 mice **(Figure 5B and 5C).** After habituation in the customized apparatus (Figure 5D),
235 control mice exhibited quick heat defense by running to the comfortable zone when
236 placed in the hot zone edge (43˚C) **(Figure 5D)**. However, optic inhibition of $LPB^{CCK}$
237 neurons led to a significant delay in the heat defense behavior, with a substantially
238 increased time in the uncomfortable zone, compared to the controls (EYFP
239 14.66%±4.119% versus GtACR1 57.3% ± 14.33%), accompanied by a much longer
240 latency returning to the comfortable zone (EYFP 22.23 ± 13.06 s versus GtACR1 163.5
241 ± 45.75 s), suggesting a delayed response to the hot stimuli **(Figure 5E-G)**. Our data
242 suggest that $LPB^{CCK}$ neurons are required to induce heat defensive behavior.

243

244 **Photostimulation of LPB$^{CCK}$-PVN neurons triggers defensive-like flight-to-nest**

245 **behavior**

246 To further investigate whether activation of the LPB$^{CCK}$-PVN pathway induces

247 defensive-like flight-to-nest behavior, we unilaterally injected Cre-dependent adeno-

248 associated virus (AAV-CAG-DIO-ChR2-EYFP or AAV-CAG-DIO-EYFP) into the

249 LPB of CCK-Cre mice and positioned an optical fiber above the PVN **(Figure 6A and**

250 **6B)**. By photostimulating the axonal terminals of LPB$^{CCK}$ neurons in the PVN, we also

251 observed apparent defensive-like flight-to-nest behavior (latency: EYFP 73.43 ± 21.08

252 s versus ChR2 8 ± 1.047 s; speed: EYFP 122.3% ± 17.81% versus ChR2 277.9% ±

253 32.85%; time in the nest: EYFP 3.751% ± 1.23% versus ChR2 89.29% ± 10.71%)

254 **(Figure 6C-H)**, similar to soma activation. Immunostaining of c-fos further verified the

255 activation of PVN neurons upon optic stimulation of axonal terminals of LPB$^{CCK}$

256 neurons **(Figure 6I-J)**. As well, terminal activation also increased heart rate and plasma

257 corticosterone levels **(Figure 6K-L)**, suggesting that PVN is an important downstream

258 target region mediating defensive-like flight-to-nest behavior and accompanying

259 activation of autonomic nervous system.

260

261 **PVN is required for defensive response to threatening situations**

262 Since LPB$^{CCK}$ neurons project to multiple regions **(Supplementary figure 1)**, thus the

263 effects observed above may arise from other downstream targets. To test the possibility,

264 we investigated whether inhibition of the PVN is required for the LPB$^{CCK}$ neurons-

265 induced defensive-like flight-to-nest behavior. To achieve this aim, we used a dual-
266 virus mediated optogenetic and chemogenetic strategy, by injecting the photoactivable
267 virus AAV2/9-DIO-ChR2-EYFP into the LPB, and a chemogenetic-inhibitory virus
268 AAV2/9-hsyn-hM4Di-mCherry into the PVN of CCK-Cre mice. By putting an optical
269 fiber above the PVN, we were able to activate the $LPB^{CCK}$ terminals and induce
270 defensive-like flight-to-nest behavior as shown above **(Figure 7A and 7B)**. Upon CNO
271 administration to inhibit PVN neurons, however, we observed a much longer latency,
272 lower speed of the mice in returning to the nest, and lower percentage of hiding time
273 spent in the nest after photostimulation of $LPB^{CCK}$-PVN pathway (latency: saline 8.286
274 ± 1.475 s versus CNO 27.86 ± 6.978 s; speed: saline 289.3% ± 25.22% versus CNO
275 111.7% ± 17.38%; time in the nest: saline 81.55% ± 11.16% versus CNO 25.6% ±
276 10.33%) **(Figure 7C-F)**. These data suggest that PVN is essential for the $LPB^{CCK}$
277 neurons activation-induced defensive-like flight-to-nest behavior.

278 $LPB^{CCK}$ neurons may release either glutamate or CCK to induce the defensive
279 behavior. To determine which neurotransmitter or modulator is engaged in the above
280 responses, we combined pharmacology with optogenetic manipulation. Two types of
281 CCK receptors are present in the central nervous system and CCKaR is widely
282 distributed throughout the PVN, whereas the expression of CCKbR receptors in PVN
283 is low **(Figure 7G-H)**. We infused glutamate receptor antagonists (CNQX + AP5),
284 CCK receptor antagonists (Devazepide + L-365,260), or artificial cerebrospinal fluid
285 (aCSF) through an implanted cannula 30-min before optogenetic activation of $LPB^{CCK}$
286 neurons **(Fig 7I-J)**. We found that blocking glutamate receptors induced a longer

latency, slower speed returning to the nest and lower percentage of hiding time in the nest, compared with ACSF-treated mice. However, blocking CCK receptors showed no significant difference compared to the control **(Figure 7K-N).** These results suggest that glutamatergic transmission from $LPB^{CCK}$ neurons to PVN regulates defensive-like flight-to-nest behavior.

**Photostimulation of $PVN^{Vglut2}$ neurons rather than $PVN^{CRH}$ neurons triggers defensive-like flight-to-nest behavior**

Of note, PVN neurons are mostly glutamatergic (Vong et al., 2011; Xu et al., 2013). We further assessed whether optogenetic activation of $PVN^{Vglut2}$ neurons elicit defensive-like behavior. We injected a Cre-dependent adeno-associated virus (AAV-CAG-DIO-ChR2-EYFP or AAV-CAG-DIO-EYFP) into the PVN and positioned an optical fiber above the PVN of Vglut2-Cre mice **(Figure 8A-B)**. We found that optogenetic activation of ChR2-expressing Vglut2 neurons in the PVN also induced defensive-like flight-to-nest behavior. Mice escaped to the nest (latency: EYFP 127.5 ± 22.5 s versus ChR2 12.83 ± 2.937 s; speed: EYFP 142.4 ± 32.07% versus ChR2 384.4% ± 83.52%), followed by longer time stay in the nest (EYFP 0.2783% ± 0.2783% versus ChR2 61.11% ± 17.58%) **(Figure 8C-E)**, compared to the control. These data suggest that optogenetic activation of $PVN^{Vglut2}$ neurons was sufficient to evoke defensive-like flight-to-nest behavior.

Recently, a study showed $PVN^{CRH}$ neurons could predict the occurrence of defensive behavior in mice (Daviu et al., 2020). To determine whether activation of the

309 $PVN^{CRH}$ neurons induced defensive-like flight-to-nest behavior, we injected a Cre-
310 dependent adeno-associated virus (AAV-CAG-DIO-ChR2-EYFP or AAV-CAG-DIO-
311 EYFP) into the PVN and positioned an optical fiber above the PVN of CRH-Cre mice
312 **(Figure 8F-G)**. However, we found that optogenetic activation of ChR2-expressing
313 CRH neurons in the PVN did not elicit defensive-like flight-to-nest behavior **(Figure**
314 **8H-J)** (latency: EYFP 77 ± 20.69 s versus ChR2 90.17 ± 22.03 s; speed: EYFP 156.6 ±
315 22.59% versus ChR2 217.2% ± 61.54%; time in the nest: EYFP 20.95% ± 13.89%
316 versus ChR2 35.28% ± 20.48%).
317
318
319
320
321
322
323
324
325
326
327
328
329
330
331
332
333

## Discussion

In the present study, we found that $LPB^{CCK}$ neurons regulate defensive-like flight-to-nest behavior through a glutmatergic excitatory projections to PVN. Morover, photoactivation of $PVN^{Vglut2}$ neurons, rather than $PVN^{CRH}$ neurons, elicits flight-to-nest behavior. Taken together, these results revealed that a novel circuit from the brainstem to hypothalamus regulates defensive behaviors **(Figure 9)**.

CCK-expressing neurons are widely distributed throughout the brain. Previous studies showed that CCK neurons in the cortex and hippocampus are mainly GABAergic (Liu et al., 2020; X. C. Sun et al., 2020; Whissell et al., 2015), while $LPB^{CCK}$ neurons are mainly glutamatergic neurons. Furthermore, $LPB^{CCK}$ neurons are anatomically separated from $LPB^{CGRP}$ neurons, which have been associated with learned fear responses and freezing behaviors, a passive coping strategy, when encountered with threats (Han et al., 2015; Keay & Bandler, 2001). By contrast, we show that selective activation of $LPB^{CCK}$ neurons triggered defensive-like flight-to-nest behavior (Keay & Bandler, 2001), an active coping strategy. Our data suggest that different neuronal subpopulations in spatially segregated regions within the LPB may encode distinct threat signals and drive distinct defensive responses when animals encounter danger. Whether $LPB^{CCK}$ neurons are further related to conditioned fear, needs further exploration.

LPB neurons are involved in regulating a series of physiological activities to protect the body from threat, including extremely heat and cold (Geerling et al., 2016; Kobayashi & Osaka, 2003; Nakamura & Morrison, 2008, 2010). Studies have demonstrated that LPB contains thermosensory neurons that facilitate various

357 homeostatic functions (Chiang et al., 2019). Recently, it has been shown that several
358 neuropeptide-containing neurons in the LPB including cholecystokinin, prodynorphin
359 and proenkephalin neurons, are activated by warm temperature (Norris et al., 2021;
360 Yang et al., 2020). Their projections to the POA are involved in maintaining temperature
361 homeostasis by driving physiological or behavioral heat defenses. In this study, we
362 show that $LPB^{CCK}$ neurons are required for the heat-induced defensive behavior,
363 suggesting that they are likely to encode heat-related threat signals and drive defensive
364 responses.

365 LPB receives diverse sources of inputs and sends projections to many forebrain
366 regions (cortex, central amygdala, BNST), hypothalamus (PVN, POA, dorsomedial
367 hypothalamic nuclei, lateral hypothalamic area), hindbrain regions (nucleus of the
368 solitary tract and spinal dorsal horn) (Chiang et al., 2019; Cooper Jr & Blumstein, 2015;
369 Ellard & Eller, 2009; Han et al., 2015; Krout & Loewy, 2000; L. Sun et al., 2020).
370 Despite many early studies mapping downstream nuclei for LPB neurons, our study is
371 the first to demonstrate that $LPB^{CCK}$ neurons possess direct anatomical and functional
372 connections with PVN neurons. We further show that $LPB^{CCK}$ neurons convey
373 threatening signals to the PVN that drives the flight-to-nest behavior. Interestingly,
374 blocking glutamate receptors rather than CCK receptors in the PVN, paired with
375 photoactivation of $LPB^{CCK}$-PVN pathway, suppressed the flight-to-nest behavior,
376 demonstrating the necessity and sufficiency of $LPB^{CCK}$-PVN glutamatergic
377 transmission for defensive responses. Besides the PVN, we also observed that $LPB^{CCK}$
378 neurons project to the paraventricular thalamic nucleus (PVT), VMH and PAG, all of

379 which have been associated with aversion and/or defensive behaviors (LeDoux, 2012;
380 Vianna et al., 2001; Wang et al., 2015). It would be interesting to further investigate
381 how these different downstream areas contribute to defensive responses.

382 PVN plays an essential role in modulating neuroendocrine and autonomous
383 functions (Canteras et al., 2001; Coote, 2005; Ferguson et al., 2008; Sutton et al., 2016).
384 Although earlier literatures suggest that PVN neurons are activated in response to
385 different threat stimuli by c-fos staining (Canteras et al., 2001; Faturi et al., 2014;
386 Martinez et al., 2008; Staples et al., 2008), it was unclear whether these neurons are
387 only involved in neuroendocrine responses to stress or directly regulate defensive
388 behaviors. Recently, increasing evidence demonstrated that PVN neurons play
389 important roles in defensive behaviors independent of hormonal actions (Daviu et al.,
390 2020; Mangieri et al., 2019b; Xu et al., 2019). Our results also support a role of PVN
391 neurons in mediating behavioral response of defense, as selective photostimulation of
392 $PVN^{Vglut2}$ neurons drives a rapid flight-to-nest behavior. While studies showed that
393 $PVN^{CRH}$ neurons participate in the initiation of escape behaviors upon a visual threat
394 and encode stress signals (Daviu et al., 2020), we found that photoactivation of $PVN^{CRH}$
395 neurons was insufficient to induce the flight-to-nest behavior. The following factors
396 may contribute to these discrepancies. First, despite that $PVN^{CRH}$ neurons receive inputs
397 from the LPB (Zhang et al., 2019), these neurons may not necessarily be $LPB^{CCK}$
398 neurons. Second, $PVN^{CRH}$ neurons receive inputs from multiple upstream nuclei and
399 activation of $PVN^{CRH}$ neuronal ensemble may not fully reflect the function of CRH
400 neurons in input-specific manner. Third, CRH neurons may only be involved in

initiation of escape but may not necessarily involved in the flight-to-nest behavior. Future studies using additional projection-specific approaches and more genetically defined cell tools may help resolve this problem. In addition, since PVN contains diverse neuronal types, it is likely that different subpopulations of neurons may coordinatively mediate defensive responses. It is worthwhile to further investigate which type of neurons in the PVN are involved in these responses.

Our data show that activation of $LPB^{CCK}$ neurons drive defensive and anxiety-like behaviors, eliciting an arousal and stressed state. Fear, anxiety and stress responses are closely associated with mental illnesses involving dysregulated neural circuits (Deisseroth, 2014; Jamalamadaka et al., 2020; Luthi & Luscher, 2014; Pitman et al., 2012). It is worth further investigation to examine whether alterations of the $LPB^{CCK}$-PVN pathway are implicated in these diseases, in which manipulation of this pathway might be an effective target for potential therapeutic strategy.

416 **Materials and Methods**

417 **Key resources table**

418

| Reagent type (species) or resource | Designation | Source or reference | Identifiers | Additional information |
|---|---|---|---|---|
| Strain, strain background (Mus musculus) | CCK-ires-Cre(Cck$^{tm1.1(cre)Zjh}$/J) | The Jackson Laboratory | JAX012706 | |
| Strain, strain background (Mus musculus) | CRH-ires-Cre (B6(Cg)-Crh$^{tm1(cre)Zjh}$/J | The Jackson Laboratory | JAX012704 | |
| Strain, strain background (Mus musculus) | Vglut2-ires-Cre (Slc17a6$^{tm2(cre)Lowl}$/J) | The Jackson Laboratory | JAX 016963 | |
| Strain, strain background (Mus musculus) | Ai14 (B6;129S6-Gt(ROSA)26Sor$^{tm14(CAG-tdTomato)Hze}$/J) | The Jackson Laboratory | JAX007908 | |
| Strain, strain background (Mus musculus) | Ai3; (B6.Cg-Gt (ROSA)26Sor$^{tm3(CAG-EYFP)Hze}$/J) | The Jackson Laboratory | JAX007903 | |
| Strain, strain background (Mus musculus) | C57BL6/J | Shanghai SLAC Laboratory Animal Co. Ltd | http://www.slaccas.com/ | |
| Antibody | Anti-Dsred, rabbit polyclonal | Takara | Cat# 632496 RRID: AB_10013483 | (1:800) |
| Antibody | Anti-CGRP, mouse monoclonal | Abcam | Cat# 81887 RRID: AB_1658411 | (1:800) |
| Antibody | Anti-GFP, goat polyclonal | Abcam | Cat# 5450 RRID: AB_304896 | (1:500) |
| Antibody | Anti-CRH, rabbit polyclona | Phoenix Biotech | Cat# H-019-06 | (1:500) |
| Antibody | Anti-c-fos, Guinea pig polyclonal | Synaptic Systems | Cat# 226004 RRID: AB_2619946 | (1:10000) |
| Antibody | Alexa Fluor 488 donkey anti-guinea pig IgG (H+L) | Jackson | Cat#112-486-068 RRID: AB_2617153 | (1:1000) |
| Antibody | Alexa Fluor 555 donkey anti-rabbit IgG (H+L) | Invitrogen | Cat#A31572 RRID: AB_162543 | (1:1000) |
| Antibody | Alexa Fluor 488 donkey anti-mouse | Invitrogen | Cat# R37114 RRID: AB_2556542 | (1:1000) |

| | | | | |
|---|---|---|---|---|
| | IgG (H+L) | | | |
| Antibody | Alexa Fluor 488 donkey anti-goat IgG (H+L) | Invitrogen | Cat# A11055<br>RRID: AB_2534102 | (1:1000) |
| Antibody | Alexa Fluor 488 donkey anti-rabbit IgG (H+L) | Jackson | Cat# R37118<br>RRID: AB_2556546 | (1:1000) |
| Commercial assay or kit | RNAscope Multiplex Fluorescent Reagent Kit v2 | Advanced Cell Diagnostics | Cat# 323100 | |
| Sequence-based reagent | RNAscope probe *Slc17a6* | Advanced Cell Diagnostics | accession number NM_080853.3 | probe region 1986-2998 |
| Sequence-based reagent | RNAscope probe *Slc32a1* | Advanced Cell Diagnostics | Accession number NM_009508.2 | probe region 894-2037 |
| Sequence-based reagent | RNAscope probe *CckaR* | Advanced Cell Diagnostics | accession number NM_009827.2 | probe region 328-1434 |
| Sequence-based reagent | RNAscope probe *CckbR* | Advanced Cell Diagnostics | accession number NM_007627.4 | probe region 136-1164 |
| Chemical compound, drug | CNQX disodium salt hydrate | Sigma-Aldrich | Cat#1045 | |
| Chemical compound, drug | Devazepide | Sigma-Aldrich | Cat#2304 | |
| Chemical compound, drug | Clozapine N-oxide | Sigma-Aldrich | Cat#C0832 | |
| Chemical compound, drug | L-365,260 | Sigma-Aldrich | Cat#143626 | |
| Chemical compound, drug | DAPI | Sigma-Aldrich | N/A | |
| Chemical compound, drug | Tween-20 | Sigma-Aldrich | N/A | |
| Strain, strain background (AAV2/9) | AAV2/9-hEF1a-DIO-hChR2(H134R)-EYFP-WPRE-pA | Shanghai Taitool Bioscience Co. | Cat# S0199-9 | Viral titers: 2.95x1013 particles/ml |
| Strain, strain background (AAV2/9) | AAV2/9-hEF1a-DIO-EYFP-WPRE-pA | Shanghai Taitool Bioscience Co. | Cat#S0196-9 | Viral titers:$1.0x10^{12}$ particles/ml |
| Strain, strain background | AAV2/9-CAG-DIO-hGtACR1-P2A- | Shanghai Taitool Bioscience Co. | Cat# S0311-9 | Viral titers:$5 \times 10^{13}$ particles/ml |

| | | | | |
|---|---|---|---|---|
| (AAV2/9) | EGFP-WPRE-pA | | | |
| Strain, strain background (AAV2/9) | rAAV2/9-hSyn-DIO-mGFP-2A-Synaptophysin-mRuby | Shanghai Taitool Bioscience Co. | Cat# S0250-9 | Viral titers :1.55x$10^{13}$ particles/ml |
| Strain, strain background (AAV2/2) | rAAV2/2-Retro-hEF1a-DIO-EYFP-WPRE-pA | Shanghai Taitool Bioscience Co. | Cat# S0196-2R | Viral titers: 2.52x$10^{13}$ particles/ml |
| Strain, strain background (AAV2/9) | AAV2/9-hSyn-mCherry-WPRE-pA | Shanghai Taitool Bioscience Co. | Cat# S0238-9 | Viral titers: ≥1.0x$10^{13}$ particles/ml |
| Strain, strain background (AAV2/9) | AAV2/9-hSyn-hM4D(Gi)-mCherry-WPRE-pA | Shanghai Taitool Bioscience Co. | Cat# S0279-9 | Viral titers: ≥1.0x$10^{13}$ particles/ml |
| Software, algorithm | ANY-Maze software 5.3 | Global Biotech Inc. | http://www.anymaze.co.uk/ | |
| Software, algorithm | Image J | NIH | https://imagej.nih.gov/ij/index.html;%20 RRID:SCR_003070 | |
| Software, algorithm | GraphPad Prism 6 | GraphPad Software | https://www.graphpad.com/scientificsoftware/prism/; RRID: SCR_002798 | |
| Software, algorithm | MatLab R2016a | MathWorks | https://www.mathworks.com/products.html; RRID:SCR_001622 | |

**Animals**

CCK-ires-Cre ($Cck^{tm1.1(cre)Zjh}$/J; Stock No. 012706), CRH-ires-Cre (B6(Cg)-$Crh^{tm1(cre)Zjh}$/J; Stock No. 012704), Vglut2-ires-Cre ($Slc17a6^{tm2(cre)Lowl}$/J; Stock No. 016963), Ai14 (B6;129S6-Gt(ROSA)26$Sor^{tm14(CAG-tdTomato)Hze}$/J; Stock No. 007908), C57BL/6 mice were obtained from the Shanghai Laboratory Animal Center. Adult male mice were used in our study. Mice housed at 22 ± 1 °C and 55 ± 5% humidity on a 12-hr light/12-hr dark cycle (light on from 07:00 to 19:00) with food and water ad libitum. All experimental procedures were approved by the Animal Advisory Committee at

428 Zhejiang University and were performed in strict accordance with the National
429 Institutes of Health Guidelines for the Care and Use of Laboratory Animals. All
430 surgeries were performed under sodium pentobarbital anesthesia, and every effort was
431 made to minimize suffering.
432
433 **Immunohistochemistry**
434 Animals were transcardially perfused with saline and 4% PFA. Brains were post-fixed
435 overnight in 4% PFA at 4 °C, followed by immersed in 30% sucrose. Coronal sections
436 (40 μm) were cut by a CM1950 Microtome (Leica). Immunostaining was performed as
437 previously described (Zhang et al., 2018). The brain slices were permeabilized in 0.5%
438 Triton X-100 in Tris-buffered saline, blocked with 100 mM glycine and 5% bovine
439 serum albumin (BSA) containing 5% normal donkey serum. Tissue sections were
440 subsequently incubated with diluted primary and secondary antibodies as indicated,
441 nuclei stained with 6-diamidino2-phenylindole (DAPI), and slides mounted with
442 antifade reagents. The primary antibodies used were: Guinea pig anti-c-fos (Synaptic
443 Systems, Cat# 226004), Rabbit anti-Dsred (Takara, Cat# 632496), Goat anti-GFP
444 (Abcam, Cat# 5450), Mouse anti-CGRP (Abcam, Cat# 81887). Slides were imaged
445 with a confocal microscope (Olympus FluoView FV1200).
446
447 **RNAscope in situ hybridization**
448 We used RNAscope multiplex fluorescent reagent kit and designed probes (ACDBio
449 Inc.) to perform fluorescence in situ hybridization. Mouse brain tissue was sectioned

450 into 20 μm sections by cryostat (Leica CM 1950). Then sections were mounted on slides
451 and air-dried at room temperature. Subsequently, the sections were dehydrated in 50%
452 EtOH, 70% EtOH, and 100% EtOH for 5-10 min each time and air-dried at room
453 temperature again. Thereafter, protease digestion was performed in a 40 °C HybEZ
454 oven for 30 min pretreatment, slides were hybridized with pre-warmed probe in a 40 °C
455 HybEZ oven for 2 hours. Probes used in our paper were: *Slc17a6* probe (*VgluT2,*
456 accession number NM_080853.3, probe region 1986-2998), *Slc32a1* probe (*VGAT*,
457 accession number NM_009508.2, probe region 894-2037), *CCKaR* probe (accession
458 number NM_009827.2, probe region 328-1434), *CCKbR* probe (accession number
459 NM_007627.4, probe region 136-1164). After hybridization, the brain sections went
460 through 4 steps of signal amplification fluorescent label. Anti-DsRed or GFP staining
461 was performed after the RNAscope staining. Slides were imaged with a confocal
462 microscope (Olympus FluoView FV1200).
463

464 **Stereotaxic injections and optical fiber/cannula implantation**

465 For surgical procedures, mice were anaesthetized with sodium pentobarbital (0.1 g/kg)
466 and placed in a stereotaxic apparatus (RWD). Stereotaxic surgery was performed as
467 described (Li Sun et al., 2020). Briefly, holes were made into the skull over the target
468 areas to inject the virus with glass pipettes (diameter,10-15 mm) or to implant optical
469 fibers [outer diameter (o.d.): 200 μm; length: 6.0 mm, 0.37 NA; Inper] or to implant of
470 guide cannula [outer diameter (o.d.): 0.41 mm; RWD]. The coordinates relative to
471 bregma were as follows according to the Paxinos and Franklin (2001) atlas. For all

experiments, mice with incorrect injection sites were excluded from further analysis.

For optical activation of $LPB^{CCK}$ neurons, AAV2/9-hEF1a-DIO-hChR2(H134R)-EYFP-WPRE-pA(viral titers: $2.95\times10^{13}$ particles/ml; Taitool Bioscience) or AAV2/9-hEF1a-DIO-EYFP-WPRE-pA (viral titers: $1.0\times10^{12}$ particles/ml; Taitool Bioscience) virus was unilaterally microinjected into the LPB (AP:-4.8; ML:-1.35; DV: -3.4; mm relative to bregma) of CCK-Cre mice. The virus was diluted into $5.9\times10^{12}$ genomic copies per ml with phosphate-buffered saline (PBS) before use and injected with 65 nl into the LPB. Virus was delivered at a flow rate of 10 nl/min. The glass capillary was left in place for an additional 10 min after injection to allow diffusion of the virus. The cannulas were held in place with dental cement above the LPB (AP: -4.8; ML: -1.35; DV: -3.2; mm relative to bregma).

For optical activation of $PVN^{Vglut2}$ neurons, AAV2/9-EF1a-DIO-hChR2-EYFP (viral titers: $2.95\times10^{13}$ particles/ml; Taitool Bioscience) or AAV2/9-EF1α-DIO-EYFP (viral titers: $1.0\times10^{12}$ particles/ml; Taitool Bioscience) virus was unilaterally microinjected into the PVN (AP: -0.4; ML: -0.15; DV: -4.95; mm relative to bregma) of Vglut2-Cre mice. The virus was diluted into $2.0\times10^{12}$ genomic copies per ml with PBS before use and injected with 70 nl into the PVN. Virus was delivered at a flow rate of 15 nl/min. The glass capillary was left in place for an additional 10 min after injection to allow diffusion of the virus. The cannulas were held in place with dental cement above the PVN (AP: -0.4; ML: -0.15; DV: -4.75; mm relative to bregma).

For optical activation of $PVN^{CRH}$ neurons, AAV2/9-EF1a-DIO-hChR2-EYFP (viral titers: $2.95\times10^{13}$ particles/ml; Taitool Bioscience) or AAV2/9-EF1α-DIO-EYFP

494 (viral titers: $1.0\times10^{12}$ particles/ml ; Taitool Bioscience) was unilaterally microinjected
495 into the PVN (AP: -0.4; ML: -0.15; DV: -4.90 mm relative to bregma) of CRH-Cre
496 mice. The virus was diluted into $4.0\times10^{12}$ genomic copies per ml with PBS before use
497 and injected with 75 nl into the PVN. Virus was delivered at a flow rate of 15 nl/min.
498 The glass capillary was left in place for an additional 10 min after injection to allow
499 diffusion of the virus. The cannulas were held in place with dental cement above the
500 PVN (AP: -0.4; ML: -0.15; DV: -4.7; mm relative to bregma).

501 For optical inhibition of $LPB^{CCK}$ neurons, AAV2/9-EF1α-DIO-hGtACR1-P2A-
502 eYFP-WPRE ($5\times10^{13}$ particles/ml; Taitool Bioscience) or AAV2/9-hEF1a-DIO-EYFP-
503 WPRE-pA (viral titers: $1.0\times10^{12}$ particles/ml; Taitool Bioscience) virus was bilaterally
504 infused to the LPB (AP: -4.8; ML: -1.35; DV: -3.4; mm relative to bregma) of CCK-
505 Cre mice. The virus was diluted into $1.67\times10^{12}$ genomic copies per ml with PBS before
506 use and injected with 70 nl into the LPB. Optical fibers were bilaterally implanted at an
507 angle of 5° above the LPB (AP: -4.8; ML: -1.72; DV: -2.94; mm relative to bregma).

508 In order to study the downstream of $LPB^{CCK}$ neurons, AAV2/9-hSyn-DIO-mGFP-
509 2A-Synaptophysin-mRuby (viral titers: $1.55\times10^{13}$ particles/ml; Taitool Bioscience)
510 virus was unilaterally injected into the LPB (AP: -4.8 mm; ML: -1.35 mm; DV: -3.4
511 mm) of CCK-Cre mice; in order to study the source of CCKergic upstream of PVN,
512 AAV2/2-Retro-hEF1a-DIO-EYFP-WPRE-pA (viral titers: $2.52\times10^{13}$ particles/ml;
513 Taitool Bioscience) virus was unilaterally injected into the PVN (AP, -0.4 mm; ML, -
514 0.2mm; DV, -4.85mm) of CCK-Cre mice.

515 For $LPB^{CCK}$-PVN axon terminal stimulation, AAV2/9-hEF1a-DIO-
516 hChR2(H134R)-EYFP-WPRE-pA (viral titers: $2.95\times10^{13}$ particles/ml; Taitool
517 Bioscience) or AAV2/9-hEF1a-DIO-EYFP-WPRE-pA (viral titers: $1.0\times10^{12}$
518 particles/ml; Taitool Bioscience) virus was unilaterally microinjected into the LPB (AP:
519 -4.8; ML: -1.35; DV: -3.4; mm relative to bregma) of CCK-Cre mice. The virus was
520 diluted into $5.9\times10^{12}$ genomic copies per ml with PBS before use and injected with 65
521 nl into the LPB. After the virus was expressed for 2 weeks, for $LPB^{CCK}$-PVN axon
522 terminals stimulation, optical fibers were unilaterally implanted above the PVN (AP: -
523 0.4; ML: -0.2; DV: -4.7; mm relative to bregma).
524 For pharmacological experiments (procedures of optical activation of $LPB^{CCK}$
525 neurons have been mentioned above), drug cannulas were ipsilaterally implanted into
526 the PVN (AP, -0.4 mm; ML, -0.2mm; DV, -4.7mm).
527 For prolonged inhibition of PVN neurons, AAV2/9-hSyn-mCherry-WPRE-pA
528 (viral titers: $\geq1.0\times10^{13}$ particles/ml; Taitool Bioscience) or AAV2/9-hSyn-hM4D(Gi)-
529 mCherry-WPRE-pA(viral titers: $\geq1.0\times10^{13}$ particles/ml; Taitool Bioscience) virus was
530 microinjected into the PVN (AP, -0.4 mm; ML, -0.2mm; DV, -4.85mm) of CCK-Cre
531 mice.
532
533 **In vivo optogenetic manipulation**
534 For optogenetic manipulation experiments, an implanted fiber was connected to a 473
535 nm laser power source (Newdoon Inc., Hangzhou, China). The power of the blue (473
536 nm) (Newdoon Inc., Hangzhou, China) was 0.83-3.33 mW $mm^2$ as measured at the tip

537 of the fiber. 473 nm laser (ChR2: power 5-15 mW, frequency 20 Hz, pulse width 5 ms;
538 GtACR1: power 15 mW, direct current) was supplied to activate or inhibit neurons,
539 respectively.
540

541 **Pharmacological antagonism**

542 Antagonism was delivered 30 min before optical activation of $LPB^{CCK}$ neurons. For
543 blocking glutamatergic neurotransmission, we firstly connected guiding cannula with a
544 Hamilton syringe via a polyethylene tube. Then we infused 0.25 μl mixed working
545 solution containing CNQX disodium salt hydrate (0.015 μg; Sigma-Aldrich), a
546 glutamate AMPA receptor antagonist, and AP5 (0.03 μg; Sigma-Aldrich), a NMDA
547 receptor antagonist, into the PVN with a manual microinfusion pump (RWD, 68606)
548 over 5 min. For blocking CCKergic neurotransmission, 0.25 μl mixed solution
549 containing Devazepide (0.0625 μg; Sigma-Aldrich), a CCKaR receptor antagonist, and
550 L-365,260(0.0625 μg; Sigma-Aldrich), a CCKbR receptor antagonist, was infused into
551 the PVN over a period of 5 min. To prevent backflow of fluid, the fluid-delivery cannula
552 was left for 10 min after infusion.
553

554 **Chemogenetic manipulation**

555 CNO (Sigma) was dissolved in saline (5 mg in 10 mL DMSO & 190 mL NaCl). CNO
556 was injected intraperitoneally at 0.3 mg per kg of body weight for chemogenetic
557 manipulation.
558

559 **Fos induction and analysis**

560 For c-Fos quantification, mice were perfused 1.5 h after 10 min blue photostimulation
561 illumination, and sections were cut. The boundaries of the nuclei were defined
562 according to brain atlases Mouse Brain Atlas (Franklin and Paxinos, 2008). Cell
563 counting was carried out manually using Image J-win64.

564

565 **Behavioral task**

566 For all behavioral tests, experimenters were blinded to genotypes and treatments. Mice
567 were handled daily at least seven days before performing behavioral tests. All the
568 apparatuses and cages were sequentially wiped with 70% ethanol and $ddH_2O$ then air-
569 dried between stages. At the end of behavioral tests, mice were perfused with 4% PFA
570 followed by post hoc analysis to confirm the viral injection sites, optic fiber and cannula
571 locations. Mice with incorrect viral injection sites, incorrect positioning of optical fibers
572 or cannulae were excluded.

573

574 **Flight-to-nest test**

575 Flight-to-nest test was performed using previously described methods (Zhou, Z., et al,
576 2019). Flight-to-nest test was performed in a 40×40×30 cm closed box with a 27-inch
577 LED monitor stationed on top to display the stimulus. A nest in the shape of a 20 cm
578 wide×12 cm high triangular prism was in the corner of the closed Plexiglas box. There
579 are two cameras, one from the top, one from the side (Logitech) that record the mouse's
580 activity simultaneously. Briefly, on day 1, the mice were habituated to the box

581 conditions for 15 min. On day 2, the mice were first allowed to explore the box for 5-
582 10 min. When the mice were in the corner furthest from the nest and within in a body-
583 length distance from the wall, they were given optical stimulus. For optogenetic
584 activation of $LPB^{CCK}$ neurons or $LPB^{CCK}$-PVN experiments, mice received a 20 s 473
585 nm blue laser (frequency 20 Hz, pulse width 5 ms) with 15-20 mW (terminal) or 5-10
586 mW (soma) light power at the fiber tips. For prolonged inhibition of PVN neurons,
587 Clozapine Noxide (CNO, Sigma-Aldrich) was dissolved in saline to a concentration of
588 3 mg/ml. The flight-to-nest test was performed 1.5 h after CNO intraperitoneally
589 injection.
590
591 **Flight-to-nest behavioral analysis**
592 The behaviors of the mice were recorded and analysed automatically with Anymaze
593 software (Global Biotech Inc). Behavioral analysis was performed as previously
594 described (Zhou, Z., et al, 2019). Flight-to-nest behavior was characterized on the basis
595 of the three aspects: latency to return nest, speed (% of baseline speed), time spent in
596 nest (% of 2 min). Latency to return nest refers to the moment from optical stimulus
597 onset to moment when the mouse first went into the nest. Speed (% of baseline speed)
598 refers to the ratio of the post-stimulation speed to the baseline speed. We recorded the
599 speed of the mice in the 50 seconds before photostimulation presentation as the baseline
600 speed. The post-stimulation speed was record from the time of stimulation to 15 s after.
601 It was averaged over a 1 s time window centered on the maximum speed. Time spent

in nest (% of 2 min) refers to the time from mouse's body was first completely under the shelter after photostimulation to the time when the mouse left the nest.

**Heat defense test**

For optogenetic inhibition tests exposing mice to a heat defense environment. We used a translucent plastic box (38×25 cm) divided into two parts, the smaller part is the unheated comfortable zone (5×25 cm), and the larger part with rubber heating pad is the hot uncomfortable zone (33×25 cm). The rubber heating pad was heated at 43℃, and the heat insulated pad in the comfortable zone was placed to avoid the heat. The test involves two stages, the first stage (habituation), the mouse was placed in the hot uncomfortable zone and allowed to explore the whole apparatus freely for 5 min to acclimate. The second stage (test) , the mouse was placed on the edge of the hot uncomfortable zone, while exposed to light（473 nm, 15 mw, 20 s）and allowed to explore for 5 min. In the second stage, the time spent in the hot uncomfortable zone and the latency time from the hot uncomfortable zone to the comfortable zone was calculated by Anymaze software. The heating temperature 43℃ was chosen because it would cause heat escape but not heat pain.

**Open field test**

The open-field chamber was made of plastic (50 × 50 × 50 cm). At the start of the test, mice were placed in the periphery of the open-field chamber. The open field test lasted 5 min.

**Elevated plus-maze test**

The elevated plus maze was made of plastic with two open arms (30×5 cm), two closed arms (30×5×30 cm) and a central platform (5×5×5 cm). At the beginning of the experiments, mice were placed in the centeral platform facing a closed arm. The elevated plus-maze test lasted 5 min.

**Heart rate measurements**

Heart rate was measured via a pulse oximeter (MouseOx Plus; Starr Life Sciences). Mice were placed in the home cage with a detector fixed around the neck. After habituation for 10 min, heart rate was simultaneously measured for 10 min while intermittent 2 min period blue light was applied. Each mouse was tested 3 times, and the mean heart rate was calculated. Heart rate data was analyzed with the MouseOx Plus Conscious Applications Software.

**Pupil size measurements**

Mice were adapted to constant room light (100 lx) for 1 h before testing. Mice were kept unanaesthetized and restrained in a stereotaxic apparatus during the experiment. The pupil size was recorded using Macro module camera under constant light conditions before stimulation, during stimulation, and after stimulation. The test lasted 90 s, consisting of 30 s light off-on-off epochs. The pupil size was later measured by Matlab software.

646

647 **Measurements of corticosterone**

648 Blood samples were collected to determine the hormone levels. Taking Blood was
649 performed in the morning by rapidly collecting heart blood after anesthetization. We
650 immediately collected blood after 10 min of light stimulation (10 mw, 20 Hz, 5 ms pulse
651 width, 15 s per min, 473 nm). Blood samples were temporarily placed in iced plastic
652 tubes coated with heparin. All serum was prepared after every blood sample was
653 centrifuged at 2000 g for 2.5 min at 4°C. Supernatant was collected and plasma
654 corticosterone concentration was measured using commercially-available ELISA kits
655 (Enzo ADI-900-097).

656

657 **In vitro electrophysiology**

658 Each mouse was anesthetized with pentobarbital sodium (100 mg/kg, i.p.) and
659 decapitated. Then the whole brain was quickly dissected into ice-cold oxygenated (95%
660 $O_2$ and 5% $CO_2$) artificial cerebrospinal fluid (aCSF) (93 mM N-methyl-D-glucamine,
661 2.5 mM KCl, 1.2 mM $NaH_2PO_4$, 20 mM HEPES, 25 mM D-glucose, 30 mM $NaHCO_3$,
662 10 mM $MgSO_4$, 0.5 mM $CaCl_2$, 5 mM sodium ascorbate, 3 mM sodium pyruvate, and
663 1 mM kynurenic acid), followed by cutting coronally into 300 μm slices on a microtome
664 (VTA-1200S; Leica). Slices containing the LPB were transferred to a similar solution
665 (93 mM NaCl, 2.5 mM KCl, 1.2 mM $NaH_2PO_4$, 20 mM HEPES, 25 mM D-glucose, 30
666 mM $NaHCO_3$, 2 mM $MgSO_4$, 2 mM $CaCl_2$, 5 mM sodium ascorbate, 3 mM sodium
667 pyruvate, and 1 mM kynurenic acid), and incubated for at lowest 1 h at room

temperature (24-26°C). Then the brain slices were transferred to a recording chamber attached to the fixed stage of an BX51WI microscope (Olympus) (solution containing: 125 mM NaCl, 3 mM KCl, 1.25 mM $NaH_2PO_4$, HEPES, 10 mM D-glucose, 26 mM $NaHCO_3$, 2 mM $MgSO_4$ and 2 mM $CaCl_2$). Patch glass electrodes were pulled from borosilicate capillaries (BF150-86-10; Sutter Instrument Co, Novato, CA, USA) and filled with artificial intracellular fluid following component: 135 mM $CsMeSO_3$, 10 mM HEPS, 0.5 mM EGTA, 3.3 mM QX-314, 4 mM Mg-ATP, 0.3 mM $Na_2$-GTP, 8 mM $Na_2$-Phosphocreatine. Whole-cell voltage-clamp recordings were made with a MultiClamp 700B amplifier (Molecular Devices). To tested the efficacy of ChR2-mediated activation, LED-generated blue light pulses were applied to recorded neurons using 4 different frequencies (5,10, 20, and 40 Hz). To test the effects of photoactivation of $LPB^{CCK}$ projection terminals within PVN, blue light pulses were applied to the recorded PVN neurons. To confirm that postsynaptic currents were monosynaptic, the blue light-evoked currents were recorded in the presence of ACSF (Ctrl), TTX (1 μM) and 4-AP (100 μM). To confirm that postsynaptic currents were monosynaptic. CNQX (20 μM) and AP5 (50 μM) were perfused with ACSF to examine the neurotransmitter type used on $LPB^{CCK}$-PVN projection. Signals were low-pass filtered at 10 kHz and digitized at 10 kHz (MICRO3 1401, Cambridge Electronic Design). Data were acquired and analyzed using Spike2 7.04 software (Cambridge Electronic Design).

**Quantification and statistical analysis**

All data analyses were conducted blinded. All statistical analyses were performed with

GraphPad Prism (version 7.0) and analyzed by Unpaired Student's t-tests, one-way ANOVA, two-way ANOVA according to the form of the data. Nonparametric tests were used if the data did not match assumed Gaussian distribution. Animals were randomly assigned to treatment groups. All data were presented as Mean ± SEM, with statistical significance taken as *$p < 0.05$, **$p < 0.01$ and ***$p < 0.001$.

**Acknowledgements**

We thank Weisheng Wang, Xiaoming Li, Bin Zhang, Zhi Chen, Kai Liu, Yu-dong Zhou, Huifang Lou for technical support. This work was supported by the National Key Research and Development Program (2021ZD0202700 and 2021ZD0202703), the National Natural Science Foundation of China (82090033) the NSFC-Guangdong Joint Fund (U20A6005), the Key Realm R&D Program of Guangdong province (2019B030335001), the Key Research and Development Program of Zhejiang province (2020C03009 and 2020R01001), the Research Units for Emotion and Emotion Disorders, Chinese Acedemy of Medical Sciences (2019-I2M-5-057).

**Author contributions**

Fan Wang, conceptualization, data curation, investigation, writing original draft, writing-review, revising and editing, designed the experiments, performed the experiments including immunohistochemistry, optogenetics, chemogenetics, behavioral tests, neuropharmacology, collected and analyzed the data, project administration; Yuge Chen, investigation, designed the experiments, performed the experiments including immunohistochemistry, optogenetics, behavioral tests, collected

and analyzed the data, writing-review, revising and editing; Yuxin Lin, Xuze Wang, Performed the experiments including immunohistochemistry, optogenetics, chemogenetics, behavioral tests, neuropharmacology, collected and analyzed the data, writing-review and editing; Kaiyuan Li, Jintao Wu, performed electrophysiology experiments; Yong Han, Zhenggang Zhu writing-review, and editing; Xingyi Shi, Chaoying Long, analyzed the data; Xiaojun Hu, technical support; Shumin Duan, Zhihua Gao, conceptualization, project administration， supervision, conceived and designed the experiments, funding acquisition, writing the manuscript, writing-review and editing.

**Declaration of interests**

The authors declare no competing interests.

**References**

Alhadeff, A. L., Su, Z., Hernandez, E., Klima, M. L., Phillips, S. Z., Holland, R. A., Guo, C., Hantman, A. W., De Jonghe, B. C., & Betley, J. N. (2018, Mar 22). A Neural Circuit for the Suppression of Pain by a Competing Need State. *Cell, 173*(1), 140-152 e115. DOI:10.1016/j.cell.2018.02.057

Anderson, D. J., & Adolphs, R. (2014, Mar 27). A framework for studying emotions across species. *Cell, 157*(1), 187-200. DOI:10.1016/j.cell.2014.03.003

Bertoglio, L. J., de Bortoli, V. C., & Zangrossi, H., Jr. (2007, Jul 2). Cholecystokinin-2

735 receptors modulate freezing and escape behaviors evoked by the electrical
736 stimulation of the rat dorsolateral periaqueductal gray. *Brain Res, 1156*, 133-
737 138. DOI:10.1016/j.brainres.2007.04.038
738 Blanchard, D. C., Griebel, G., & Blanchard, R. J. (2001, May). Mouse defensive
739 behaviors: pharmacological and behavioral assays for anxiety and panic.
740 *Neurosci Biobehav Rev, 25*(3), 205-218. DOI:10.1016/s0149-7634(01)00009-4
741 Campos, C. A., Bowen, A. J., Han, S., Wisse, B. E., Palmiter, R. D., & Schwartz, M. W.
742 (2017, Jul). Cancer-induced anorexia and malaise are mediated by CGRP
743 neurons in the parabrachial nucleus. *Nat Neurosci, 20*(7), 934-942.
744 DOI:10.1038/nn.4574
745 Campos, C. A., Bowen, A. J., Roman, C. W., & Palmiter, R. D. (2018, Mar 29).
746 Encoding of danger by parabrachial CGRP neurons. *Nature, 555*(7698), 617-
747 622. DOI:10.1038/nature25511
748 Canteras, N. S., Ribeiro-Barbosa, E. R., & Comoli, E. (2001, Dec). Tracing from the
749 dorsal premammillary nucleus prosencephalic systems involved in the
750 organization of innate fear responses. *Neurosci Biobehav Rev, 25*(7-8), 661-668.
751 DOI:10.1016/s0149-7634(01)00048-3
752 Carter, M. E., Soden, M. E., Zweifel, L. S., & Palmiter, R. D. (2013, Nov 7). Genetic
753 identification of a neural circuit that suppresses appetite. *Nature, 503*(7474),
754 111-114. DOI:10.1038/nature12596
755 Chen, J. Y., Campos, C. A., Jarvie, B. C., & Palmiter, R. D. (2018, Nov 21). Parabrachial
756 CGRP Neurons Establish and Sustain Aversive Taste Memories. *Neuron, 100*(4),

891-899 e895. DOI:10.1016/j.neuron.2018.09.032

Chen, L., Liu, Y., Su, P., Hung, W., Li, H., Wang, Y., Yue, Z., Ge, M. H., Wu, Z. X., Zhang, Y., Fei, P., Chen, L. M., Tao, L., Mao, H., Zhen, M., & Gao, S. (2022, Feb 8). Escape steering by cholecystokinin peptidergic signaling. *Cell Rep, 38*(6), 110330. DOI:10.1016/j.celrep.2022.110330

Chiang, M. C., Bowen, A., Schier, L. A., Tupone, D., Uddin, O., & Heinricher, M. M. (2019, Oct 16). Parabrachial Complex: A Hub for Pain and Aversion. *J Neurosci, 39*(42), 8225-8230. DOI:10.1523/JNEUROSCI.1162-19.2019

Cooper Jr, W. E., & Blumstein, D. T. (2015). *Escaping From Predators: Escape decisions prior to pursuit*. DOI:10.1017/cbo9781107447189

Coote, J. H. (2005, Mar). A role for the paraventricular nucleus of the hypothalamus in the autonomic control of heart and kidney. *Exp Physiol, 90*(2), 169-173. DOI:10.1113/expphysiol.2004.029041

Crawford, M., & Masterson, F. A. (1982, Oct-Dec). Species-specific defense reactions and avoidance learning. An evaluative review. *Pavlov J Biol Sci, 17*(4), 204-214. DOI:10.1007/BF03001275

Daviu, N., Fuzesi, T., Rosenegger, D. G., Rasiah, N. P., Sterley, T. L., Peringod, G., & Bains, J. S. (2020, Mar). Paraventricular nucleus CRH neurons encode stress controllability and regulate defensive behavior selection. *Nat Neurosci, 23*(3), 398-410. DOI:10.1038/s41593-020-0591-0

Deisseroth, K. (2014, Jan 16). Circuit dynamics of adaptive and maladaptive behaviour. *Nature, 505*(7483), 309-317. DOI:10.1038/nature12982

Dong, P., Wang, H., Shen, X. F., Jiang, P., Zhu, X. T., Li, Y., Gao, J. H., Lin, S., Huang, Y., He, X. B., Xu, F. Q., Duan, S., Lian, H., Wang, H., Chen, J., & Li, X. M. (2019, Jun). A novel cortico-intrathalamic circuit for flight behavior. *Nat Neurosci, 22*(6), 941-949. DOI:10.1038/s41593-019-0391-6

Eilam, D. (2005). Die hard: a blend of freezing and fleeing as a dynamic defense--implications for the control of defensive behavior. *Neurosci Biobehav Rev, 29*(8), 1181-1191. DOI:10.1016/j.neubiorev.2005.03.027

Ellard, C. G., & Eller, M. C. (2009, Mar). Spatial cognition in the gerbil: computing optimal escape routes from visual threats. *Anim Cogn, 12*(2), 333-345. DOI:10.1007/s10071-008-0193-9

Evans, D. A., Stempel, A. V., Vale, R., Ruehle, S., Lefler, Y., & Branco, T. (2018, Jun). A synaptic threshold mechanism for computing escape decisions. *Nature, 558*(7711), 590-594. DOI:10.1038/s41586-018-0244-6

Fanselow, M. S., & Bolles, R. C. (1979, Aug). Naloxone and shock-elicited freezing in the rat. *J Comp Physiol Psychol, 93*(4), 736-744. DOI:10.1037/h0077609

Faturi, C. B., Rangel, M. J., Jr., Baldo, M. V., & Canteras, N. S. (2014, May). Functional mapping of the circuits involved in the expression of contextual fear responses in socially defeated animals. *Brain Struct Funct, 219*(3), 931-946. DOI:10.1007/s00429-013-0544-4

Ferguson, A. V., Latchford, K. J., & Samson, W. K. (2008, Jun). The paraventricular nucleus of the hypothalamus - a potential target for integrative treatment of autonomic dysfunction. *Expert Opin Ther Targets, 12*(6), 717-727.

DOI:10.1517/14728222.12.6.717

Fulwiler, C. E., & Saper, C. B. (1984, Aug). Subnuclear organization of the efferent connections of the parabrachial nucleus in the rat. *Brain Res, 319*(3), 229-259. DOI:10.1016/0165-0173(84)90012-2

Garfield, A. S., Shah, B. P., Madara, J. C., Burke, L. K., Patterson, C. M., Flak, J., Neve, R. L., Evans, M. L., Lowell, B. B., Myers, M. G., Jr., & Heisler, L. K. (2014, Dec 2). A parabrachial-hypothalamic cholecystokinin neurocircuit controls counterregulatory responses to hypoglycemia. *Cell Metab, 20*(6), 1030-1037. DOI:10.1016/j.cmet.2014.11.006

Gauriau, C., & Bernard, J. F. (2002, Mar). Pain pathways and parabrachial circuits in the rat. *Exp Physiol, 87*(2), 251-258. DOI:10.1113/eph8702357

Geerling, J. C., Kim, M., Mahoney, C. E., Abbott, S. B., Agostinelli, L. J., Garfield, A. S., Krashes, M. J., Lowell, B. B., & Scammell, T. E. (2016, Jan 1). Genetic identity of thermosensory relay neurons in the lateral parabrachial nucleus. *Am J Physiol Regul Integr Comp Physiol, 310*(1), R41-54. DOI:10.1152/ajpregu.00094.2015

Gross, C. T., & Canteras, N. S. (2012, Sep). The many paths to fear. *Nat Rev Neurosci, 13*(9), 651-658. DOI:10.1038/nrn3301

Han, S., Soleiman, M. T., Soden, M. E., Zweifel, L. S., & Palmiter, R. D. (2015, Jul 16). Elucidating an Affective Pain Circuit that Creates a Threat Memory. *Cell, 162*(2), 363-374. DOI:10.1016/j.cell.2015.05.057

Jamalamadaka, T., Griffith, E., Steer, H., & Salkovskis, P. (2020, Sep). Fear of illness

recurrence and mental health anxiety in people recovering from psychosis and common mental health problems. *Br J Clin Psychol, 59*(3), 403-423. DOI:10.1111/bjc.12253

Kaur, S., Pedersen, N. P., Yokota, S., Hur, E. E., Fuller, P. M., Lazarus, M., Chamberlin, N. L., & Saper, C. B. (2013, May 1). Glutamatergic signaling from the parabrachial nucleus plays a critical role in hypercapnic arousal. *J Neurosci, 33*(18), 7627-7640. DOI:10.1523/JNEUROSCI.0173-13.2013

Keay, K. A., & Bandler, R. (2001, Dec). Parallel circuits mediating distinct emotional coping reactions to different types of stress. *Neurosci Biobehav Rev, 25*(7-8), 669-678. DOI:10.1016/s0149-7634(01)00049-5

Kobayashi, A., & Osaka, T. (2003, Sep). Involvement of the parabrachial nucleus in thermogenesis induced by environmental cooling in the rat. *Pflugers Arch, 446*(6), 760-765. DOI:10.1007/s00424-003-1119-7

Krout, K. E., & Loewy, A. D. (2000, Dec 18). Parabrachial nucleus projections to midline and intralaminar thalamic nuclei of the rat. *J Comp Neurol, 428*(3), 475-494. DOI:10.1002/1096-9861(20001218)428:3<475::aid-cne6>3.0.co;2-9

LeDoux, J. (2012, Mar 8). Rethinking the Emotional Brain (vol 73, pg 653, 2012). *Neuron, 73*(5), 1052-1052. DOI:10.1016/j.neuron.2012.02.018

Liu, X., Dimidschstein, J., Fishell, G., & Carter, A. G. (2020, Oct 9). Hippocampal inputs engage CCK+ interneurons to mediate endocannabinoid-modulated feed-forward inhibition in the prefrontal cortex. *Elife, 9*. DOI:10.7554/eLife.55267

Luthi, A., & Luscher, C. (2014, Dec). Pathological circuit function underlying addiction

and anxiety disorders. *Nat Neurosci, 17*(12), 1635-1643. DOI:10.1038/nn.3849

Mangieri, L. R., Jiang, Z., Lu, Y., Xu, Y., Cassidy, R. M., Justice, N., Xu, Y., Arenkiel, B. R., & Tong, Q. (2019a, Jul/Aug). Defensive Behaviors Driven by a Hypothalamic-Ventral Midbrain Circuit. *eNeuro, 6*(4). DOI:10.1523/ENEURO.0156-19.2019

Mangieri, L. R., Jiang, Z., Lu, Y., Xu, Y., Cassidy, R. M., Justice, N., Xu, Y., Arenkiel, B. R., & Tong, Q. (2019b, Jul/Aug). Defensive Behaviors Driven by a Hypothalamic-Ventral Midbrain Circuit. *eNeuro, 6*(4), ENEURO.0156-0119.2019. DOI:10.1523/ENEURO.0156-19.2019

Martinez, R. C., Carvalho-Netto, E. F., Amaral, V. C., Nunes-de-Souza, R. L., & Canteras, N. S. (2008, Oct 10). Investigation of the hypothalamic defensive system in the mouse. *Behav Brain Res, 192*(2), 185-190. DOI:10.1016/j.bbr.2008.03.042

Mu, D., Deng, J., Liu, K. F., Wu, Z. Y., Shi, Y. F., Guo, W. M., Mao, Q. Q., Liu, X. J., Li, H., & Sun, Y. G. (2017, Aug 18). A central neural circuit for itch sensation. *Science, 357*(6352), 695-699. DOI:10.1126/science.aaf4918

Nakamura, K., & Morrison, S. F. (2008, Jan). A thermosensory pathway that controls body temperature. *Nat Neurosci, 11*(1), 62-71. DOI:10.1038/nn2027

Nakamura, K., & Morrison, S. F. (2010, May 11). A thermosensory pathway mediating heat-defense responses. *Proc Natl Acad Sci U S A, 107*(19), 8848-8853. DOI:10.1073/pnas.0913358107

Norris, A. J., Shaker, J. R., Cone, A. L., Ndiokho, I. B., & Bruchas, M. R. (2021, Mar

5). Parabrachial opioidergic projections to preoptic hypothalamus mediate behavioral and physiological thermal defenses. *Elife, 10*. DOI:10.7554/eLife.60779

O'Shea, R. D., & Gundlach, A. L. (1993, Dec). Regulation of cholecystokinin receptors in the hypothalamus of the rat: reciprocal changes in magnocellular nuclei induced by food deprivation and dehydration. *J Neuroendocrinol, 5*(6), 697-704. DOI:10.1111/j.1365-2826.1993.tb00542.x

Perusini, J. N., & Fanselow, M. S. (2015, Sep). Neurobehavioral perspectives on the distinction between fear and anxiety. *Learn Mem, 22*(9), 417-425. DOI:10.1101/lm.039180.115

Pitman, R. K., Rasmusson, A. M., Koenen, K. C., Shin, L. M., Orr, S. P., Gilbertson, M. W., Milad, M. R., & Liberzon, I. (2012, Nov). Biological studies of post-traumatic stress disorder. *Nat Rev Neurosci, 13*(11), 769-787. DOI:10.1038/nrn3339

Salay, L. D., Ishiko, N., & Huberman, A. D. (2018, May). A midline thalamic circuit determines reactions to visual threat. *Nature, 557*(7704), 183-189. DOI:10.1038/s41586-018-0078-2

Shang, C., Chen, Z., Liu, A., Li, Y., Zhang, J., Qu, B., Yan, F., Zhang, Y., Liu, W., Liu, Z., Guo, X., Li, D., Wang, Y., & Cao, P. (2018, Mar 26). Divergent midbrain circuits orchestrate escape and freezing responses to looming stimuli in mice. *Nat Commun, 9*(1), 1232. DOI:10.1038/s41467-018-03580-7

Shang, C., Liu, Z., Chen, Z., Shi, Y., Wang, Q., Liu, S., Li, D., & Cao, P. (2015, Jun 26).

BRAIN CIRCUITS. A parvalbumin-positive excitatory visual pathway to trigger fear responses in mice. *Science, 348*(6242), 1472-1477. DOI:10.1126/science.aaa8694

Silva, B. A., Mattucci, C., Krzywkowski, P., Murana, E., Illarionova, A., Grinevich, V., Canteras, N. S., Ragozzino, D., & Gross, C. T. (2013, Dec). Independent hypothalamic circuits for social and predator fear. *Nat Neurosci, 16*(12), 1731-1733. DOI:10.1038/nn.3573

Staples, L. G., McGregor, I. S., Apfelbach, R., & Hunt, G. E. (2008, Feb 19). Cat odor, but not trimethylthiazoline (fox odor), activates accessory olfactory and defense-related brain regions in rats. *Neuroscience, 151*(4), 937-947. DOI:10.1016/j.neuroscience.2007.11.039

Sun, L., Liu, R., Guo, F., Wen, M. Q., Ma, X. L., Li, K. Y., Sun, H., Xu, C. L., Li, Y. Y., Wu, M. Y., Zhu, Z. G., Li, X. J., Yu, Y. Q., Chen, Z., Li, X. Y., & Duan, S. (2020, Nov 25). Parabrachial nucleus circuit governs neuropathic pain-like behavior. *Nat Commun, 11*(1), 5974. DOI:10.1038/s41467-020-19767-w

Sun, X. C., Bernstein, M. J., Meng, M. Z., Rao, S. Y., Sorensen, A. T., Yao, L., Zhang, X. H., Anikeeva, P. O., & Lin, Y. X. (2020, Apr 16). Functionally Distinct Neuronal Ensembles within the Memory Engram. *Cell, 181*(2), 410-+. DOI:10.1016/j.cell.2020.02.055

Sutton, A. K., Myers, M. G., Jr., & Olson, D. P. (2016). The Role of PVH Circuits in Leptin Action and Energy Balance. *Annu Rev Physiol, 78*(1), 207-221. DOI:10.1146/annurev-physiol-021115-105347

Tovote, P., Esposito, M. S., Botta, P., Chaudun, F., Fadok, J. P., Markovic, M., Wolff, S. B., Ramakrishnan, C., Fenno, L., Deisseroth, K., Herry, C., Arber, S., & Luthi, A. (2016, Jun 9). Midbrain circuits for defensive behaviour. *Nature, 534*(7606), 206-212. DOI:10.1038/nature17996

Tovote, P., Meyer, M., Ronnenberg, A., Ogren, S. O., Spiess, J., & Stiedl, O. (2005). Heart rate dynamics and behavioral responses during acute emotional challenge in corticotropin-releasing factor receptor 1-deficient and corticotropin-releasing factor-overexpressing mice. *Neuroscience, 134*(4), 1113-1122. DOI:10.1016/j.neuroscience.2005.05.027

Uddin, O., Studlack, P., Akintola, T., Raver, C., Castro, A., Masri, R., & Keller, A. (2018, Jan-Jul). Amplified parabrachial nucleus activity in a rat model of trigeminal neuropathic pain. *Neurobiol Pain, 3*, 22-30. DOI:10.1016/j.ynpai.2018.02.002

Vianna, D. M., Landeira-Fernandez, J., & Brandão, M. L. (2001, Dec). Dorsolateral and ventral regions of the periaqueductal gray matter are involved in distinct types of fear. *Neurosci Biobehav Rev, 25*(7-8), 711-719. DOI:10.1016/s0149-7634(01)00052-5

Vong, L., Ye, C., Yang, Z., Choi, B., Chua, S., Jr., & Lowell, B. B. (2011, Jul 14). Leptin action on GABAergic neurons prevents obesity and reduces inhibitory tone to POMC neurons. *Neuron, 71*(1), 142-154. DOI:10.1016/j.neuron.2011.05.028

Wang, L., Chen, I. Z., & Lin, D. (2015, Mar 18). Collateral pathways from the ventromedial hypothalamus mediate defensive behaviors. *Neuron, 85*(6), 1344-1358. DOI:10.1016/j.neuron.2014.12.025

Wang, W., Schuette, P. J., La-Vu, M. Q., Torossian, A., Tobias, B. C., Ceko, M., Kragel, P. A., Reis, F. M., Ji, S., Sehgal, M., Maesta-Pereira, S., Chakerian, M., Silva, A. J., Canteras, N. S., Wager, T., Kao, J. C., & Adhikari, A. (2021, Sep 1). Dorsal premammillary projection to periaqueductal gray controls escape vigor from innate and conditioned threats. *Elife, 10*. DOI:10.7554/eLife.69178

Wang, W., Schuette, P. J., Nagai, J., Tobias, B. C., Cuccovia, V. R. F. M., Ji, S., de Lima, M. A. X., La-Vu, M. Q., Maesta-Pereira, S., Chakerian, M., Leonard, S. J., Lin, L., Severino, A. L., Cahill, C. M., Canteras, N. S., Khakh, B. S., Kao, J. C., & Adhikari, A. (2021, Jun 2). Coordination of escape and spatial navigation circuits orchestrates versatile flight from threats. *Neuron, 109*(11), 1848-1860 e1848. DOI:10.1016/j.neuron.2021.03.033

Wei, P., Liu, N., Zhang, Z., Liu, X., Tang, Y., He, X., Wu, B., Zhou, Z., Liu, Y., Li, J., Zhang, Y., Zhou, X., Xu, L., Chen, L., Bi, G., Hu, X., Xu, F., & Wang, L. (2015, Apr 9). Processing of visually evoked innate fear by a non-canonical thalamic pathway. *Nat Commun, 6*, 6756. DOI:10.1038/ncomms7756

Whissell, P. D., Cajanding, J. D., Fogel, N., & Kim, J. C. (2015, Sep 23). Comparative density of CCK- and PV-GABA cells within the cortex and hippocampus. *Frontiers in Neuroanatomy, 9*, 124. DOI:ARTN 124
10.3389/fnana.2015.00124

Xu, Y., Lu, Y., Cassidy, R. M., Mangieri, L. R., Zhu, C., Huang, X., Jiang, Z., Justice, N. J., Xu, Y., Arenkiel, B. R., & Tong, Q. (2019, Aug 1). Identification of a neurocircuit underlying regulation of feeding by stress-related emotional

955 responses. *Nat Commun, 10*(1), 3446. DOI:10.1038/s41467-019-11399-z

956 Xu, Y., Wu, Z., Sun, H., Zhu, Y., Kim, E. R., Lowell, B. B., Arenkiel, B. R., Xu, Y., &
957 Tong, Q. (2013, Dec 3). Glutamate mediates the function of melanocortin
958 receptor 4 on Sim1 neurons in body weight regulation. *Cell Metab, 18*(6), 860-
959 870. DOI:10.1016/j.cmet.2013.11.003

960 Yang, H., Yang, J., Xi, W., Hao, S., Luo, B., He, X., Zhu, L., Lou, H., Yu, Y. Q., Xu, F.,
961 Duan, S., & Wang, H. (2016, Feb). Laterodorsal tegmentum interneuron
962 subtypes oppositely regulate olfactory cue-induced innate fear. *Nat Neurosci,*
963 *19*(2), 283-289. DOI:10.1038/nn.4208

964 Yang, W. Z., Du, X., Zhang, W., Gao, C., Xie, H., Xiao, Y., Jia, X., Liu, J., Xu, J., Fu,
965 X., Tu, H., Fu, X., Ni, X., He, M., Yang, J., Wang, H., Yang, H., Xu, X. H., &
966 Shen, W. L. (2020, Sep). Parabrachial neuron types categorically encode
967 thermoregulation variables during heat defense. *Sci Adv, 6*(36).
968 DOI:10.1126/sciadv.abb9414

969 Yilmaz, M., & Meister, M. (2013, Oct 21). Rapid innate defensive responses of mice to
970 looming visual stimuli. *Curr Biol, 23*(20), 2011-2015.
971 DOI:10.1016/j.cub.2013.08.015

972 Zhang, B., Wang, W., Zhang, Z., Hu, Y., Meng, F., Wang, F., Lou, H., Zhu, L., Godbout,
973 R., Duan, S., & Gao, Z. (2018, Oct 1). Alternative Splicing of Disabled-1
974 Controls Multipolar-to-Bipolar Transition of Migrating Neurons in the
975 Neocortex. *Cereb Cortex, 28*(10), 3457-3467. DOI:10.1093/cercor/bhx212

976 Zhang, S., Lv, F., Yuan, Y., Fan, C., Li, J., Sun, W., & Hu, J. (2019). Whole-Brain

Mapping of Monosynaptic Afferent Inputs to Cortical CRH Neurons. *Front Neurosci, 13*, 565. DOI:10.3389/fnins.2019.00565–

Zhou, Z., Liu, X., Chen, S., Zhang, Z., Liu, Y., Montardy, Q., Tang, Y., Wei, P., Liu, N., Li, L., Song, R., Lai, J., He, X., Chen, C., Bi, G., Feng, G., Xu, F., & Wang, L. (2019, Aug 7). A VTA GABAergic Neural Circuit Mediates Visually Evoked Innate Defensive Responses. *Neuron, 103*(3), 473-488 e476. DOI:10.1016/j.neuron.2019.05.027

987 **Figure Legends**

988 **Figure 1.** $CCK^+$ neurons in the LPB project to the PVN. **(A)** Scheme of viral strategy
989 for retrograde tracing from the PVN in CCK-Cre mice using AAV2-Retro virus. **(B)**
990 CCK-Cre mice were injected with AAV2-Retro-EYFP virus at the PVN. And traced
991 neurons ($EYFP^+$) in the LPB, PAG; scale bar, 100 μm; n=3 mice. **(C)** A heatmap
992 demonstrating the distribution of $EYFP^+$ neurons in the MO, CC, DI, PAG. The number
993 of cells in individual areas are color coded as indicated; n = 3 mice. **(D)** Scheme of viral
994 strategy for anterograde tracing from $LPB^{CCK}$ neurons using AAV-hSyn-FLEX-mGFP-
995 2A-Synaptophysin-mRuby virus. **(E)** Representative histological images of AAV-hSyn-
996 FLEx-mGFP-2A-Synaptophysin-mRuby virus expression in the CCK neurons in the
997 LPB; scale bar, 100 μm. **(F)** $LPB^{CCK}$ neurons have projections to the PVN; scale bar,
998 100 μm. The right panel shows a magnified view of rectangular part; scale bar, 100 μm;
999 n=3 mice.

1000

1001 **Figure 2.** $CCK^+$ neurons in the LPB are mostly glutamatergic neurons and send
1002 glutamatergic projections to the PVN. **(A)** Schematic of mice crossing to generate a
1003 CCK-ires-Cre::Ai14 mouse line. **(B)** Representative coronal section images illustrating
1004 the expression of CCK-tdT in the LPB; scale bar, 100 μm. **(C)** Quantification of CCK-
1005 tdT cells across the rostral-to-caudal extent of the LPB; n=3 mice. **(D)** Representative
1006 images showing co-labeling (arrowheads) of Vglut2-positive (Green) and CCK-tdT
1007 expressing cells in the LPB. Rightmost panel, magnification of the box-shaped area in
1008 the left panel (white dashed lines). Blue, DAPI staining. Scale bar, 100 μm. **(E)**

1009 Example images showing Vgat-positive (Green) and CCK-tdT-expressing cells in the
1010 LPB. Rightmost panel, magnification of the boxed area in the left panel. Blue, DAPI
1011 staining. Scale bar, 100 μm. **(F)** Representative image from a CCK-ires-Cre::Ai14
1012 mouse in the LPB region stained with antibodies against CGRP. Rightmost panels,
1013 magnification of the boxed areas in the left panels. Blue, DAPI staining. Scale bar, 100
1014 μm. **(G)** Percentage of CCK-positive neurons that co-localized with markers; n=4 mice.
1015 **(H)** Schematic of recording from PVN cells following optogenetic activation of
1016 $LPB^{CCK}$ axonal terminals. **(I-J)** Representative traces of light-evoked EPSCs recorded
1017 from PVN neurons following light stimulation of $LPB^{CCK}$ axonal terminals in the
1018 presence of ACSF(Ctrl), TTX (1 μM) and 4- AP (100 μM). Representative traces of
1019 light-evoked EPSCs recorded from PVN neurons following light stimulation of $LPB^{CCK}$
1020 axonal terminals in the presence of CNQX (20 μM) and AP5 (50 μM) (n = 9 neurons).
1021 **(K)** Quantification of excitatory postsynaptic currents (EPSCs) and inhibitory
1022 postsynaptic currents (IPSCs) from identified PVN neurons receiving inputs from the
1023 $LPB^{CCK}$ neurons.
1024
1025 **Figure 3.** Activation of $LPB^{CCK}$ neurons triggers defensive-like flight-to-nest behavior.
1026 **(A)** Left, schematic of light stimulation of and patch-clamp recording from ChR2-EYFP
1027 expressing CCK neurons in the LPB. Right, example of action potentials evoked by
1028 optogenetic stimulation $LPB^{CCK}$ neurons from using whole cell patch-clamp slice
1029 recording. **(B)** Schematic diagram of optogenetic activation of $LPB^{CCK}$ neurons. **(C)**
1030 Representative image showing the ChR2-EYFP expression and optical fiber tip

1031 locations in LPB of a CCK-Cre mouse. Scale bar, 100 μm. **(D)** Schematic of the timing
1032 and behavioral paradigm of flight-to-nest behavior test. **(E)** Experimental apparatus:
1033 Open field with a nest in the corner. **(F)** Schematic of the timing and behavioral
1034 paradigm with optical activation of $LPB^{CCK}$ neurons. **(G)** Optogenetic activation of
1035 $LPB^{CCK}$ neurons induced defensive-like flight-to-nest behavior. Mice movements were
1036 tracked in the experimental apparatus. **(H-J)** Compared with control group, ChR2 group
1037 showed shorter latency, higher speed back into the nest and higher percentage of hiding
1038 time spent in the nest (EYFP: n =7 mice, ChR2: n =7 mice; for latency, $p = 0.0006$, U
1039 = 0; Mann-Whitney test; for speed, $p = 0.0016$, $t = 4.052$, $df = 12$; unpaired t test; for
1040 time in the nest, $p < 0.0001$, $t = 19.82$, $df = 12$; unpaired t test).
1041
1042 **Figure 4.** Photostimulation of $LPB^{CCK}$ neurons induces anxiety-like behavior and
1043 autonomic responses. **(A)** Schematic of behavioral test protocol. OFT, open field test;
1044 EPM, elevated plus maze test. **(B)** Movement traces of a control group mouse (AAV2/9-
1045 EF1a-DIO-EYFP, left) and an experimental group mouse (AAV2/9-EF1a-DIO-ChR2-
1046 EYFP, right) in the open field. **(C)** Quantification of the total distance moved, time
1047 spent in center and total number of center entries in the open field tests before (Pre) and
1048 after (Post) photostimulation of $LPB^{CCK}$ neurons in CCK-Cre mice.(EYFP: n = 7 mice,
1049 ChR2: n = 7 mice; for total distance, Pre-light EYFP vs. Post-light EYFP ns $p > 0.9999$,
1050 Post-light EYFP vs. Post-light ChR2 ns $p = 0.2236$, Pre-light ChR2 vs. Post-light ChR2
1051 ns $p = 0.9026$; two-way ANOVA, Bonferroni's multiple comparisons test; for center
1052 time, Pre-light EYFP vs. Post-light EYFP ns $p > 0.9999$, Post-light EYFP vs. Post-light

ChR2 **p < 0.01 p=0.005, Pre-light ChR2 vs. Post-light ChR2 **p < 0.01 p = 0.005; two-way ANOVA, Bonferroni's multiple comparisons test; for center entries, Pre-light EYFP vs. Post-light EYFP ns p > 0.9999, Post-light EYFP vs. Post-light ChR2 ***p < 0.0005 p = 0.0004, Pre-light ChR2 vs. Post-light ChR2 **p < 0.01 p = 0.0042; two-way ANOVA, Bonferroni's multiple comparisons test). **(D)** Example traces of a control group mouse (AAV2/9-EF1a-DIO-EYFP, left) and an experimental group mouse (AAV2/9-EF1a-DIO-EYFP, right) in the elevated plus maze. **(E)** Quantification of the open arm time and open arm entries in the elevated plus maze tests before (Pre) and after (Post) photostimulation of $LPB^{CCK}$ neurons in CCK-Cre mice. (EYFP: n = 7 mice, ChR2: n = 7 mice; for open arm time, Pre-light EYFP vs. Post-light EYFP ns p > 0.9999, Post-light EYFP vs. Post-light ChR2 **p < 0.01 p = 0.0053, Pre-light ChR2 vs. Post-light ChR2 ***p<0.0005 p = 0.0005; two-way ANOVA, Bonferroni's multiple comparisons test; for open arm entries, Pre-light EYFP vs. Post-light EYFP ns p > 0.9999, Post-light EYFP vs. Post-light ChR2 **p < 0.01 p = 0.0159, Pre-light ChR2 vs. Post-light ChR2 ****p < 0.0001; two-way ANOVA, Bonferroni's multiple comparisons test). **(F)** Relative heart rate changes induced by photostimulation of $LPB^{CCK}$ neurons. (EYFP: n = 7 mice, ChR2: n = 7 mice; p = 0.0006, t = 4.603, df = 12; unpaired t test). **(G)** Schematic of detection of pupil size. **(H)** Example image of computer-detected pupil before, during and after photo stimulation of $LPB^{CCK}$ neurons. **(I)** Relative pupil size (during photostimulation/before photostimulation) of $LPB^{CCK}$ neurons. (EYFP: n = 6 mice, ChR2: n = 6 mice; p = 0.0022, U = 0; Mann-Whitney test). **(J)** Cartoon of the arousal state during the activation of $LPB^{CCK}$ neurons. **(K)** Serum

1075 corticosterone levels in EYFP and ChR2 groups. (EYFP: n = 5 mice, ChR2: n = 5 mice;
1076 p = 0.0121, t = 3.23, df = 8; unpaired t test).
1077
1078 **Figure 5.** Optogenetic inhibition of $LPB^{CCK}$ neurons suppressed heat-evoked defensive
1079 behavior. **(A)** Left, schematic of light stimulation of and patch-clamp recording from
1080 GtACR1-expressing CCK neurons in the LPB. Right, example of action potentials
1081 evoked by optogenetic inhibition of $LPB^{CCK}$ neurons from using whole cell patch-
1082 clamp slice recording. **(B)** Schematic diagram of optogenetic inhibition of $LPB^{CCK}$
1083 neurons. **(C)** Representative image showing the GtACR1-EYFP expression in the LPB
1084 and optical fiber tip locations above the LPB of a CCK-Cre mouse. **(D)** Heat defense
1085 apparatus: a translucent plastic box divided into two parts, the smaller part is the
1086 unheated comfortable zone, and the larger part with rubber heating pad is the hot
1087 uncomfortable zone. **(E)** Schematic of the timing and behavioral paradigm of heat-
1088 evoked defensive behavioral test. **(F-G)** Photoinhibition of $LPB^{CCK}$ neurons suppressed
1089 heat-evoked defensive behavior. Compared with control group, GtACR1 group showed
1090 longer latency and lower percentage of time spent in the hot zone (EYFP: n = 8 mice,
1091 GtACR1: n = 7 mice; for latency, p = 0.0059, U = 2; Mann-Whitney test; for time in
1092 the nest, p = 0.02, U = 8; Mann-Whitney test).
1093
1094 **Figure 6.** Photostimulation of $LPB^{CCK}$-PVN pathway induces defensive-like flight-to-
1095 nest behavior. **(A)** Schematic diagram of optogenetic activation of $LPB^{CCK}$-PVN
1096 neurons. **(B)** Left, Representative image showing the ChR2-EYFP expression in the

LPB of a CCK-Cre mouse. Right, Optical fiber tip locations in the PVN from a ChR2-EYFP expressing CCK-Cre mouse. **(C)** Experimental apparatus: Open field with nest in the corner. **(D)** Schematic of the timing and behavioral paradigm with optical activation of $LPB^{CCK}$-PVN. **(E)** Optogenetic activation of $LPB^{CCK}$-PVN induced defensive-like flight-to-nest behavior. Mice movements were tracked in the experimental apparatus. **(F-H)** Optogenetic activation of $LPB^{CCK}$-PVN induced defensive-like flight-to-nest behavior. Compared with control group, ChR2 group showed shorter latency, higher speed back into the nest and higher percentage of hiding time spent in the nest (EYFP: n = 7 mice, ChR2: n = 7 mice; for latency, p = 0.0012, U = 0; Mann-Whitney test; for speed, p = 0.0013, t = 4.163, df = 12; unpaired t test; for time in the nest, p = 0.0006, U = 0; Mann-Whitney test). **(I)** C-fos expression in the PVN with blue light activation of LPB-originating dio-EYFP (left) or ChR2-EYFP (right) expressing terminals in the PVN. Scale bar: 100 μm. **(J)** Quantification of c-fos positive cells in the PVN following ChR2 activation (EYFP: n = 3 mice, ChR2: n = 3 mice; p = 0.0033, t = 6.253, df = 4; unpaired t test). **(K)** Relative heart rate in mice with and without $LPB^{CCK}$-PVN projection stimulation (EYFP: n = 7 mice, ChR2: n = 7 mice; P = 0.0002, t = 5.249, df = 12; unpaired t test). **(L)** Serum corticosterone levels in EYFP and ChR2 groups. (EYFP: n = 5 mice, ChR2: n = 5 mice; P = 0.0079, U = 0; Mann-Whitney test).

**Figure 7.** PVN, as a downstream nuclei of $LPB^{CCK}$ neurons, is involved in defensive-like flight-to-nest behavior. **(A)** Schematics of experimental setup. CCK-Cre mice with

AAV2/9-DIO-ChR2-EYFP virus delivery to the LPB, AAV2/9-hsyn-hM4Di-mCherry virus delivery to the PVN, and optic fiber implantation targeting PVN were used for flight- to-nest behavior test. **(B)** Left, representative image showing the ChR2-EYFP expression in the LPB of a CCK-Cre mouse. Scale bar, 100 μm. Right, representative image showing the hM4Di-mCherry expression in the PVN and optic fiber placement in the PVN from a ChR2-EYFP expressing mouse. **(C)** Schematic of behavioral test protocol. **(D-F)** Chemogenetic inhibition of PVN neurons before optical activation of $LPB^{CCK}$-PVN showed longer latency and lower speed returning to the nest and lower percentage of hiding time spent in the nest (saline: n = 7 mice, CNO: n = 7 mice; for latency, $p = 0.0012$, $U = 1$; Mann-Whitney test; for speed, $p < 0.0001$, $t = 5.798$, $df = 12$; unpaired t test; for time in the nest, $p = 0.0031$, $t = 3.68$, $df = 12$; unpaired t test). **(G-H)** Expression of CCKaR and CCKbR throughout the PVN. Representative histological images showing CCKaR (left) and CCKbR (right) in the PVN. **(I)** Schematics of experimental setup. Optogenetic activation of $LPB^{CCK}$-PVN with a cannula implanted in the PVN for aCSF or CNQX + AP5 or Devazepide + L-365,260 delivery. Scale bar, 100 μm. **(J)** Left, representative image showing the ChR2-EYFP expression in the LPB of a CCK-Cre mouse. Scale bar, 100 μm. Right, representative image showing the cannula placement in the PVN from a ChR2-EYFP expressing CCK-Cre mouse. Scale bar, 100 μm. **(K)** Schematic of behavioral test protocol. **(L-N)** Compared with the ACSF group, microinjection of the glutamatergic receptor antagonist rather than CCK receptor antagonist into the PVN showed longer latency returning to the nest and no change in the speed back into the nest and percentage of

hiding time spent in the nest (ACSF: n = 6 mice, CNQX + AP5: n = 6 mice, Devazepide + L-365260: n = 5 mice; for latency, F (2,14) =7.658, p=0.057; One-way ANOVA; for speed, F (2,14) = 11.49, p = 0.0011; for time in the nest, One-way ANOVA; F (2,14) =16.44, p = 0.0002; One-way ANOVA).

**Figure 8.** Photoactivation of $PVN^{Vglut2}$ neurons rather than $PVN^{CRH}$ neurons triggers defensive-like flight-to-nest behavior. **(A)** Schematic diagram of optogenetic activation of $PVN^{Vglut2}$ neurons. **(B)** Representative image showing the ChR2-EYFP expression and optical fiber tip locations in the PVN of a Vglut2-Cre mouse. Scale bar, 100 μm. **(C-E)** Optogenetic activation of $PVN^{Vglut2}$ neurons induced defensive-like flight-to-nest behavior. Compared with control group, ChR2 group showed shorter latency, higher speed back into the nest and higher percentage of hiding time spent in the nest. (EYFP: n = 6 mice, ChR2: n = 6 mice; for latency, p = 0.0065, u = 2; Mann-Whitney test; for speed, p = 0.0221, t = 2.705, df = 10; unpaired t test; for time in the nest, p = 0.022, u = 0; Mann-Whitney test). **(F)** Schematic diagram of optogenetic activation of $PVN^{CRH}$ neurons. **(G)** Representative image showing the ChR2-EYFP expression and optical fiber tip locations in the PVN of a CRH-Cre mouse. Scale bar, 100 μm. **(H-J)** Optogenetic activation of $PVN^{CRH}$ neurons did not induce flight-to-nest behavior. Compared with control group, ChR2 group showed no changes in latency, speed back into the nest and total percentage of hiding time spent in the nest (EYFP: n = 5 mice, ChR2: n = 6 mice; for latency, p = 0.6664, t = 0.4456, df = 9; unpaired t test; for speed, p = 0.0221, t = 2.705, df = 10; unpaired t test; for time in the nest, p = 0.2088, t = 1.367,

df = 8; unpaired t test).

**Figure 9.** Schematic diagram of the working model. Graphical summary. These studies suggest a novel circuit that mediates defensive-like flight-to-nest behavior.

**Supplementary figure legends**

**Figure 1-figure supplement 1.** Upstream nuclei of $LPB^{CCK}$ neurons in the whole brain. **(A-D)** CCK-Cre mice with PVN delivery AAV2-Retro-EYFP virus and $EYFP^{+}$ neurons in the MO, CC, DI, PAG; scale bar, 100 μm; n = 3 mice.

**Figure1-figure supplement 2. (A-I)** Projection mapping from $LPB^{CCK}$ neurons. Representative images showing projections from $LPB^{CCK}$ neurons in the median preoptic nucleus (MnPO), lateral preoptic area (LPO), paraventricular thalamic nucleus (PVT), ventromedial hypothalamic nucleus (VMH), ventral posteromedial thalamic nucleus (VPM), lateral posterior thalamic nucleus, mediorostral part (LPMR), parasubthalamic nucleus (PSTh), PAG, deep gray layer of the superior colliculus (DpG）(n = 3 mice; green, GFP; red, mrubby; blue, DAPI). Scale bar, 100 μm; n = 3 mice.

**Source data files**

**Figure 1-source data 1.** Data for Figure 1. The number of $EYFP^{+}$ neurons in the MO, CC, DI, PAG, LPB.

1185 **Figure 2-source data 1.** Data for Figure 2. Quantification of CCK-tdT cells across the
1186 rostral-to-caudal extent of the LPB; Percentage of CCK-positive neurons that co-
1187 localized with markers; Quantification of excitatory postsynaptic currents (EPSCs) and
1188 inhibitory postsynaptic currents (IPSCs) from identified PVN neurons.
1189 **Figure 3-source data 1.** Data for Figure 3. Values for latency, speed back into the nest
1190 and percentage of hiding time spent in the nest during flight-to-nest behavior test.
1191 **Figure 4-source data 1.** Data for Figure 4. Quantification of the total distance moved,
1192 time spent in center and total number of center entries in the open field tests;
1193 Quantification of the open arm time and open arm entries in the elevated plus maze
1194 tests; Values for relative heart rate changes; Values for relative pupil size; Values for
1195 serum corticosterone levels in EYFP and ChR2 groups.
1196 **Figure 5-source data 1.** Data for Figure 5. Values for suppressed heat-evoked
1197 defensive behavior.
1198 **Figure 6-source data 1.** Data for Figure 6. Values for latency, speed back into the nest
1199 and percentage of hiding time spent in the nest during flight-to-nest behavior test;
1200 Quantification of c-fos positive cells in the PVN; Values for relative heart rate; Values
1201 for serum corticosterone levels in EYFP and ChR2 groups.
1202 **Figure 7-source data 1.** Data for Figure 7. Values for latency, speed back into the nest
1203 and percentage of hiding time spent in the nest during flight-to-nest behavior test;
1204 **Figure 8-source data 1.** Data for Figure 8. Values for latency, speed back into the nest
1205 and percentage of hiding time spent in the nest during flight-to-nest behavior test.
1206

1207 **Figure 1**

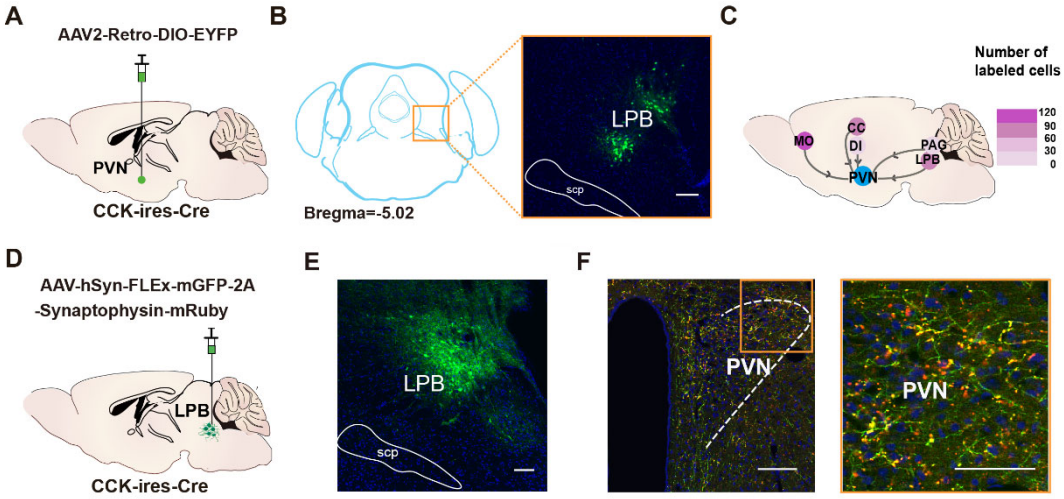


1208

1209

1210

1211

1212

1213

1214

1215

1216

1217

1218

1219

1220

1221

1222

**Figure 2**

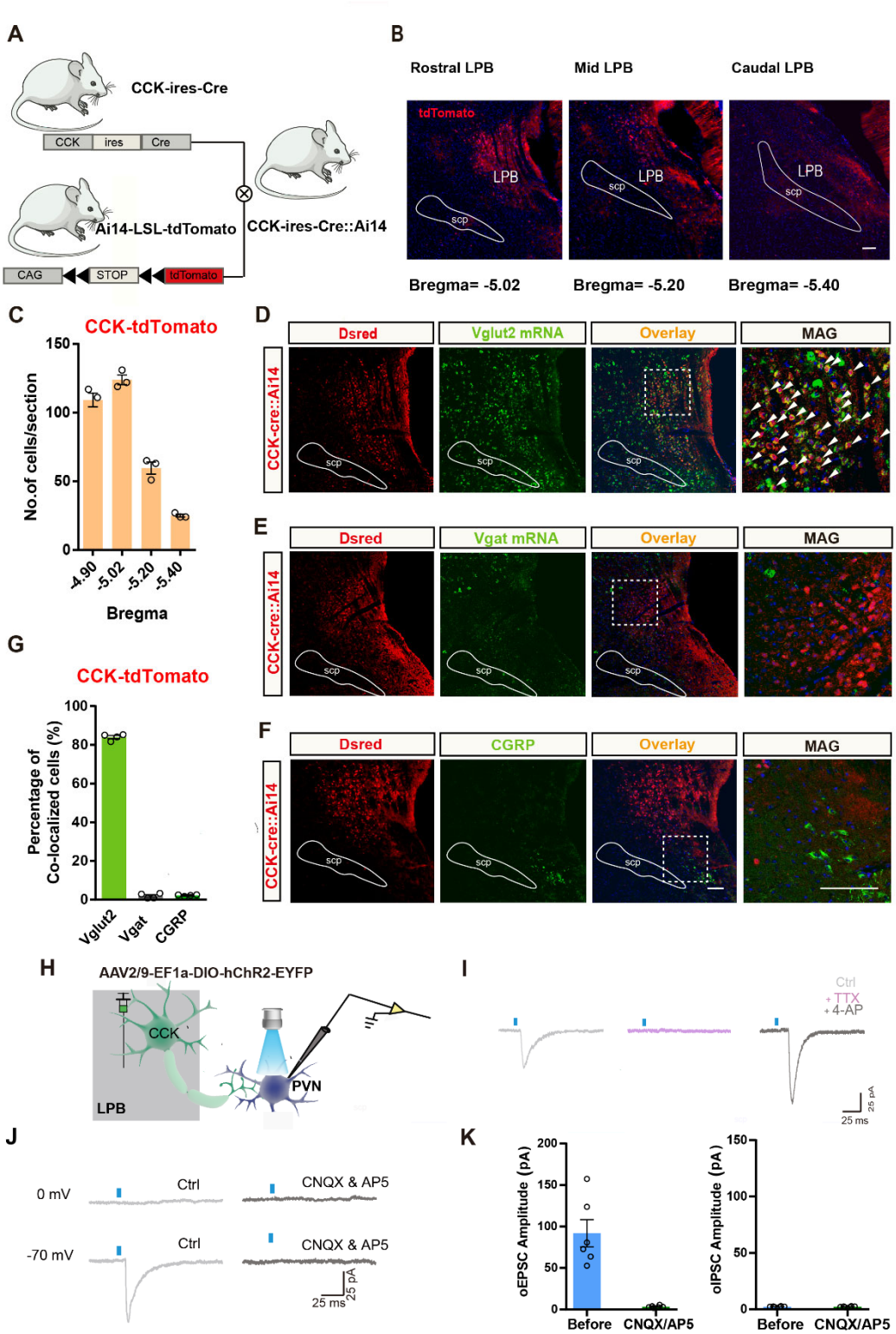
A
CCK-ires-Cre
CCK
ires
Cre
Ai14-LSL-tdTomato
CCK-ires-Cre::Ai14
CAG
STOP
tdTomato
B
Rostral LPB
Mid LPB
Caudal LPB
tdTomato
LPB
scp
Bregma= -5.02
Bregma= -5.20
Bregma= -5.40
C
CCK-tdTomato
No.of cells/section
Bregma
-4.90
-5.02
-5.20
-5.40
D
Dsred
Vglut2 mRNA
Overlay
MAG
CCK-cre::Ai14
E
Vgat mRNA
F
CGRP
G
Percentage of Co-localized cells (%)
Vglut2
Vgat
CGRP
H
AAV2/9-EF1a-DIO-hChR2-EYFP
CCK
PVN
LPB
I
Ctrl
+ TTX
+ 4-AP
25 pA
25 ms
J
0 mV
-70 mV
Ctrl
CNQX & AP5
K
oEPSC Amplitude (pA)
oIPSC Amplitude (pA)
Before
CNQX/AP5

1228 **Figure 3**

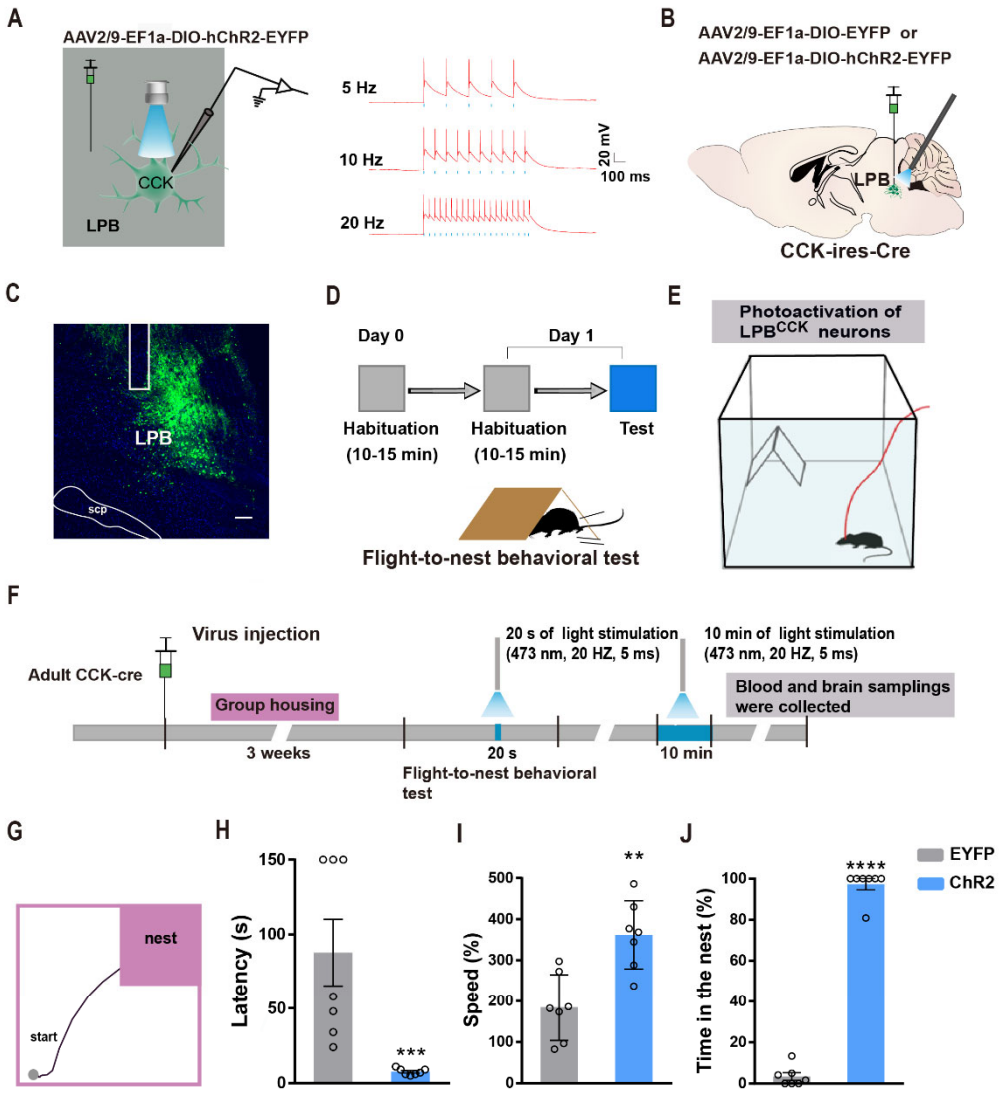


1229

1230

1231

**Figure 4**

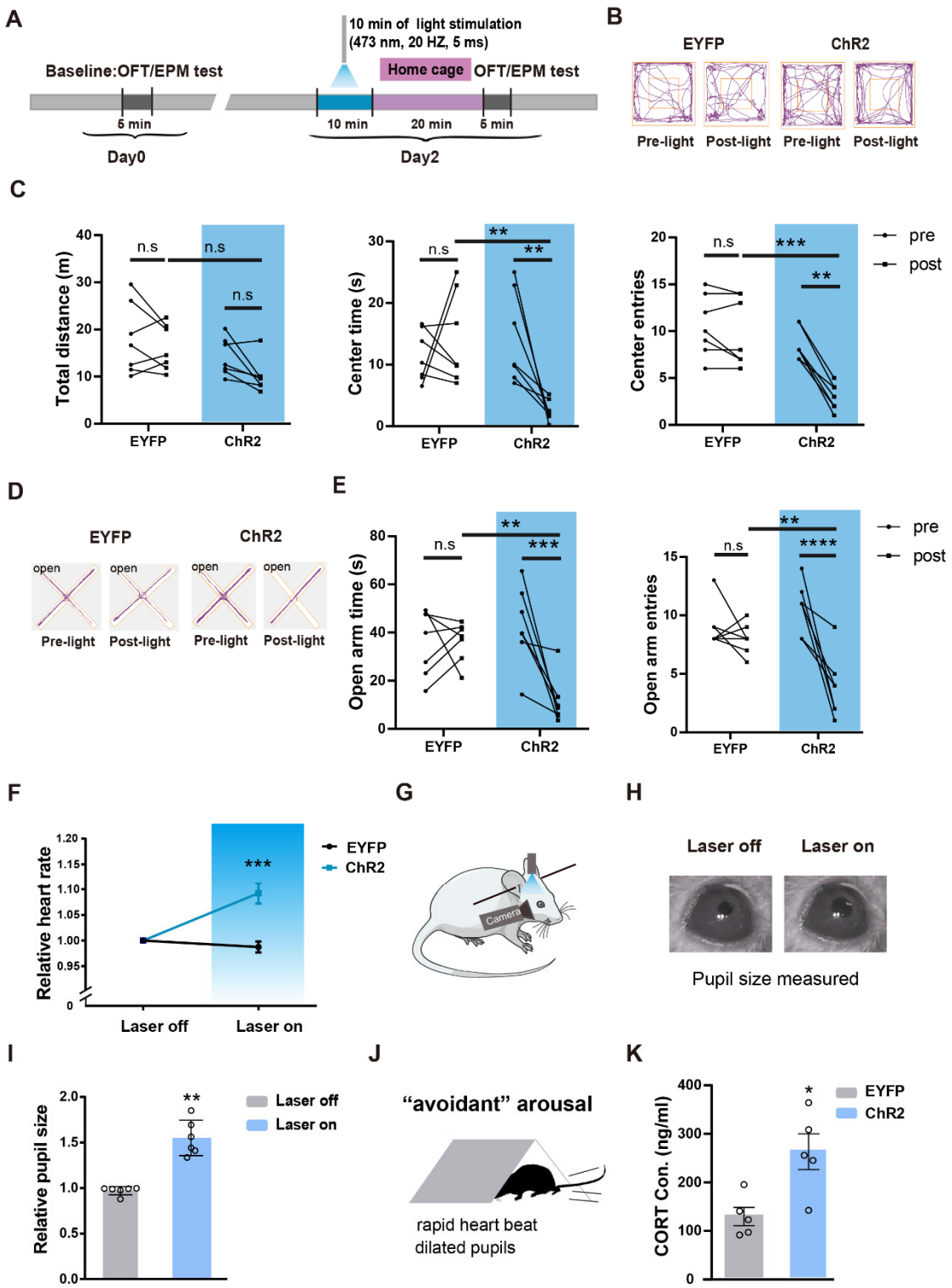
A
10 min of light stimulation
(473 nm, 20 HZ, 5 ms)
Baseline:OFT/EPM test
Home cage
OFT/EPM test
5 min
10 min
20 min
5 min
Day0
Day2
B
EYFP
ChR2
Pre-light
Post-light
Pre-light
Post-light
C
Total distance (m)
Center time (s)
Center entries
n.s
**
***
pre
post
EYFP
ChR2
D
EYFP
ChR2
open
Pre-light
Post-light
Pre-light
Post-light
E
Open arm time (s)
Open arm entries
****
F
Relative heart rate
Laser off
Laser on
G
Camera
H
Laser off
Laser on
Pupil size measured
I
Relative pupil size
J
"avoidant" arousal
rapid heart beat
dilated pupils
K
CORT Con. (ng/ml)

**Figure 5**

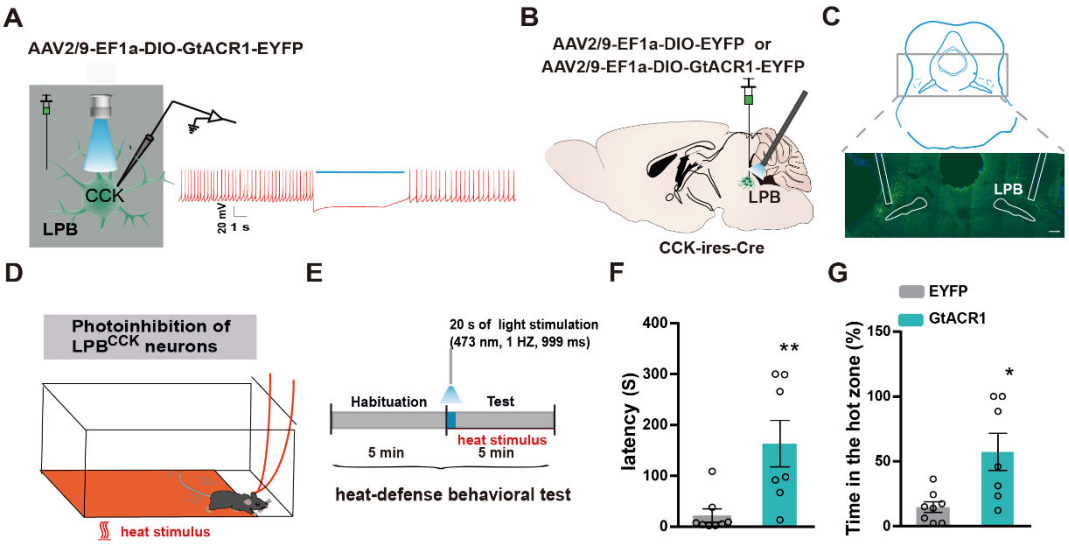
A
AAV2/9-EF1a-DIO-GtACR1-EYFP
CCK
LPB
20 mV
1 s
B
AAV2/9-EF1a-DIO-EYFP or
AAV2/9-EF1a-DIO-GtACR1-EYFP
LPB
CCK-ires-Cre
C
LPB
D
Photoinhibition of
LPBCCK neurons
heat stimulus
E
20 s of light stimulation
(473 nm, 1 HZ, 999 ms)
Habituation
Test
heat stimulus
5 min
5 min
heat-defense behavioral test
F
latency (S)
400
300
200
100
0
**
G
EYFP
GtACR1
Time in the hot zone (%)
150
100
50
0
*

1251 **Figure 6**

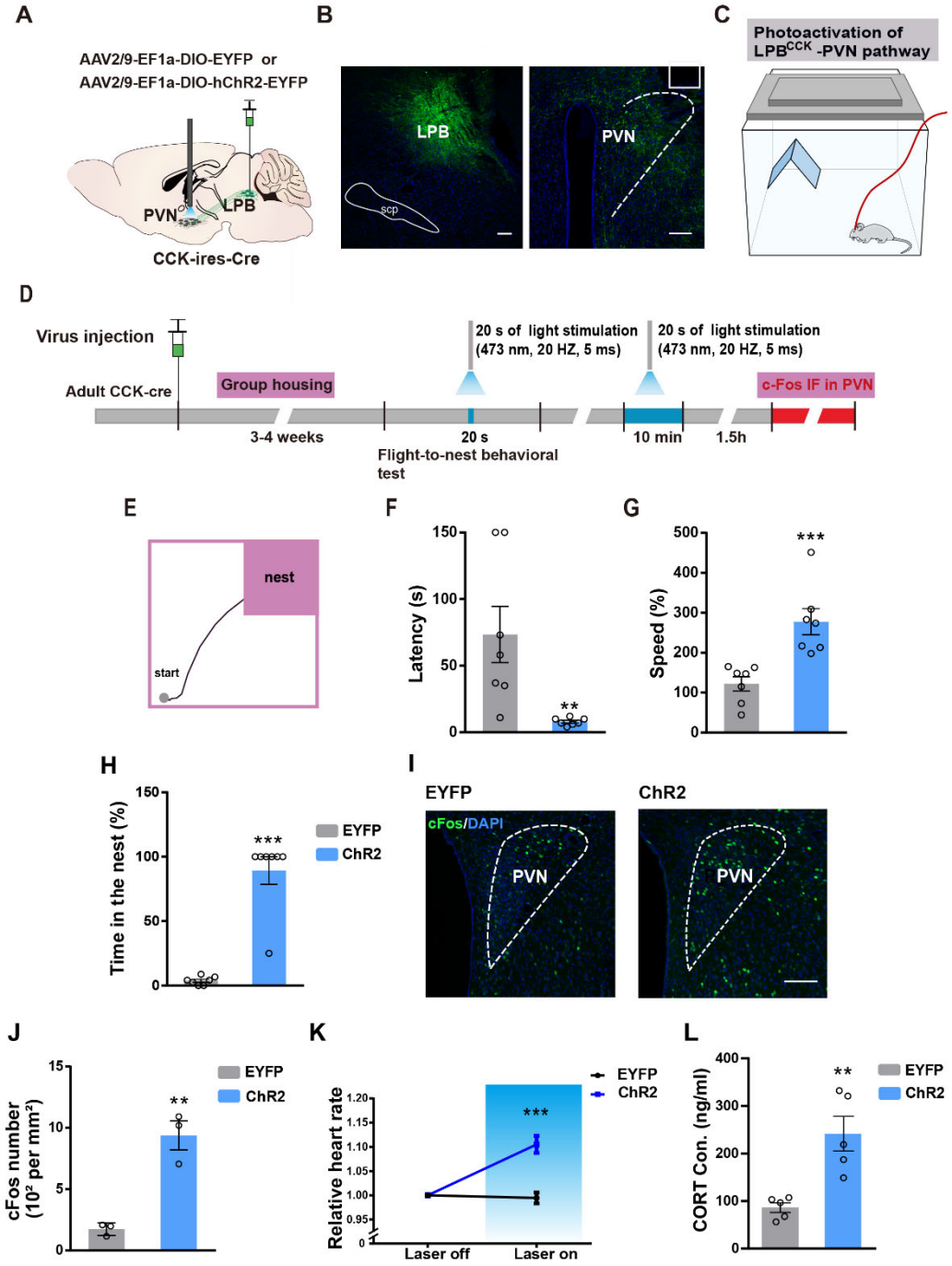


1252

1253

1254

1255 **Figure 7**

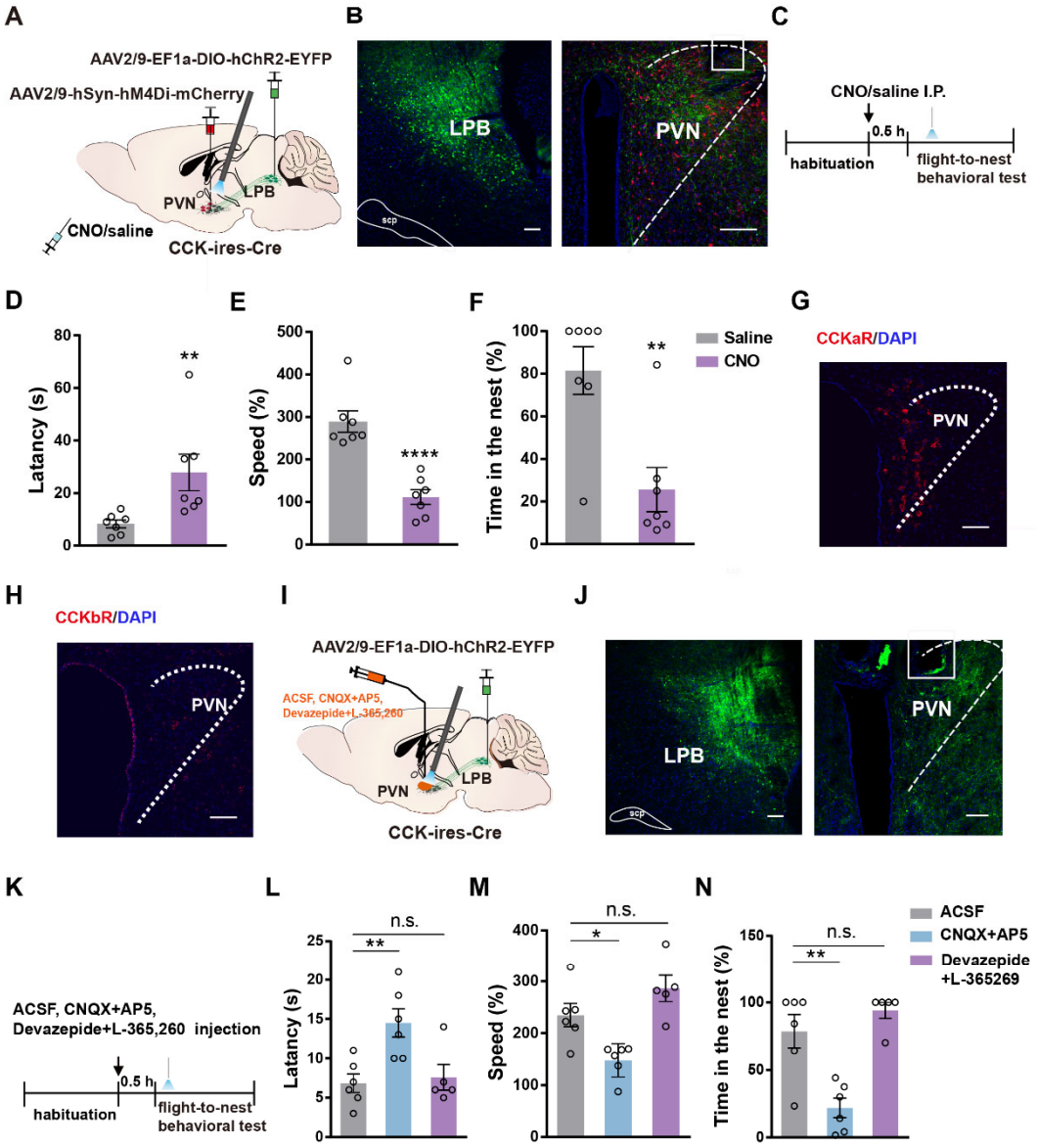


1256

1257

1258

**Figure 8**

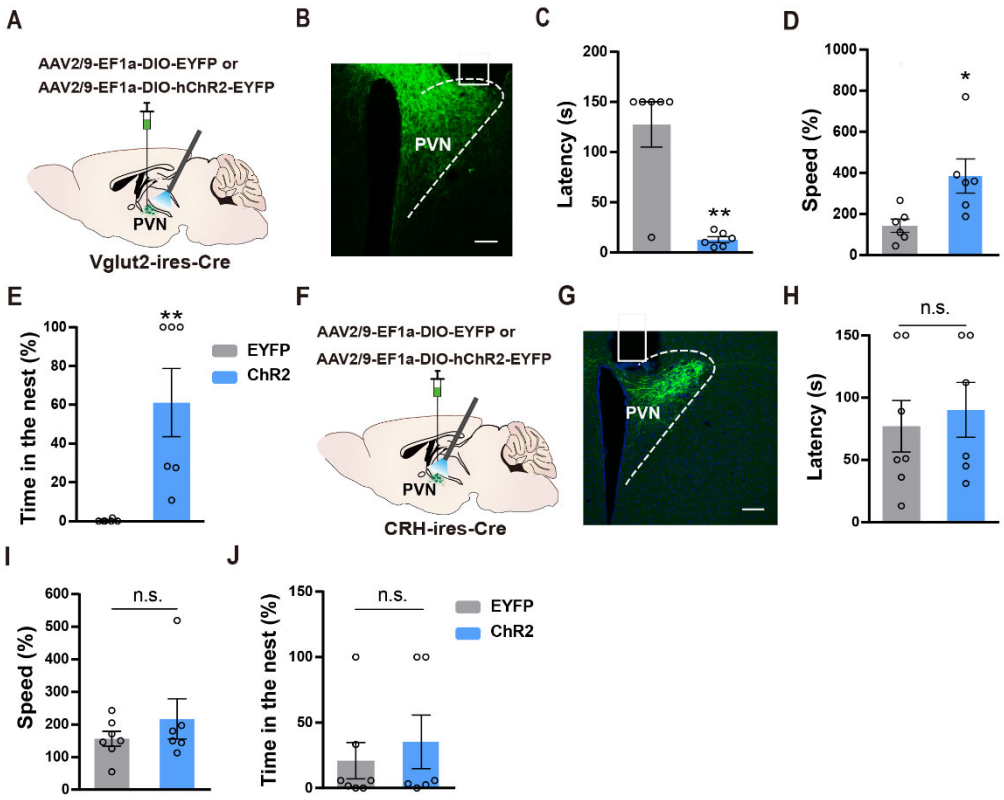
A
AAV2/9-EF1a-DIO-EYFP or
AAV2/9-EF1a-DIO-hChR2-EYFP
PVN
Vglut2-ires-Cre
B
PVN
C
Latency (s)
D
Speed (%)
E
Time in the nest (%)
EYFP
ChR2
F
AAV2/9-EF1a-DIO-EYFP or
AAV2/9-EF1a-DIO-hChR2-EYFP
PVN
CRH-ires-Cre
G
PVN
H
n.s.
Latency (s)
I
n.s.
Speed (%)
J
n.s.
Time in the nest (%)
EYFP
ChR2

**Figure 9**

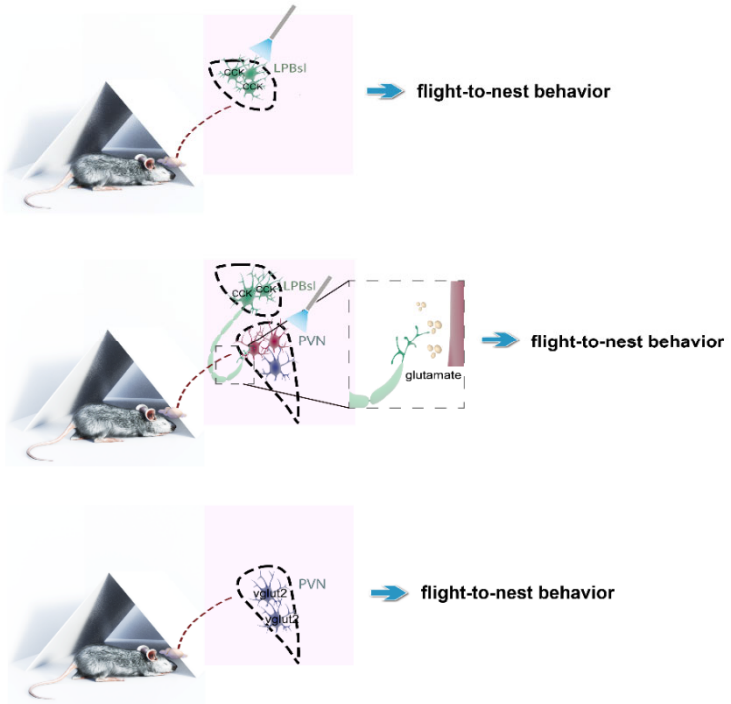
cck
cck
LPBsl
flight-to-nest behavior
cck
cck
LPBsl
PVN
glutamate
flight-to-nest behavior
PVN
vglut2
vglut2
flight-to-nest behavior

1277 **Figure 1–figure supplement 1**

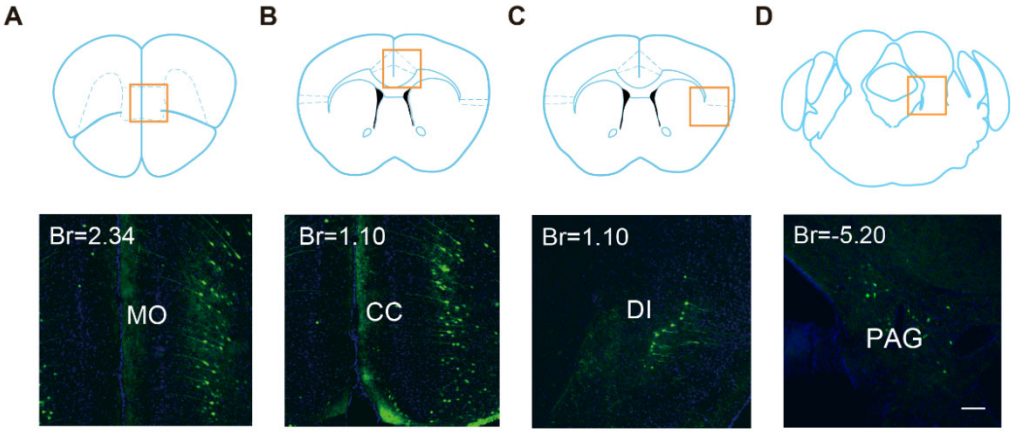


1278

1279

1280

1281

1282

1283

1284

1285

1286

1287

1288

1289

1290

1291

1292 **Figure 1–figure supplement 2**

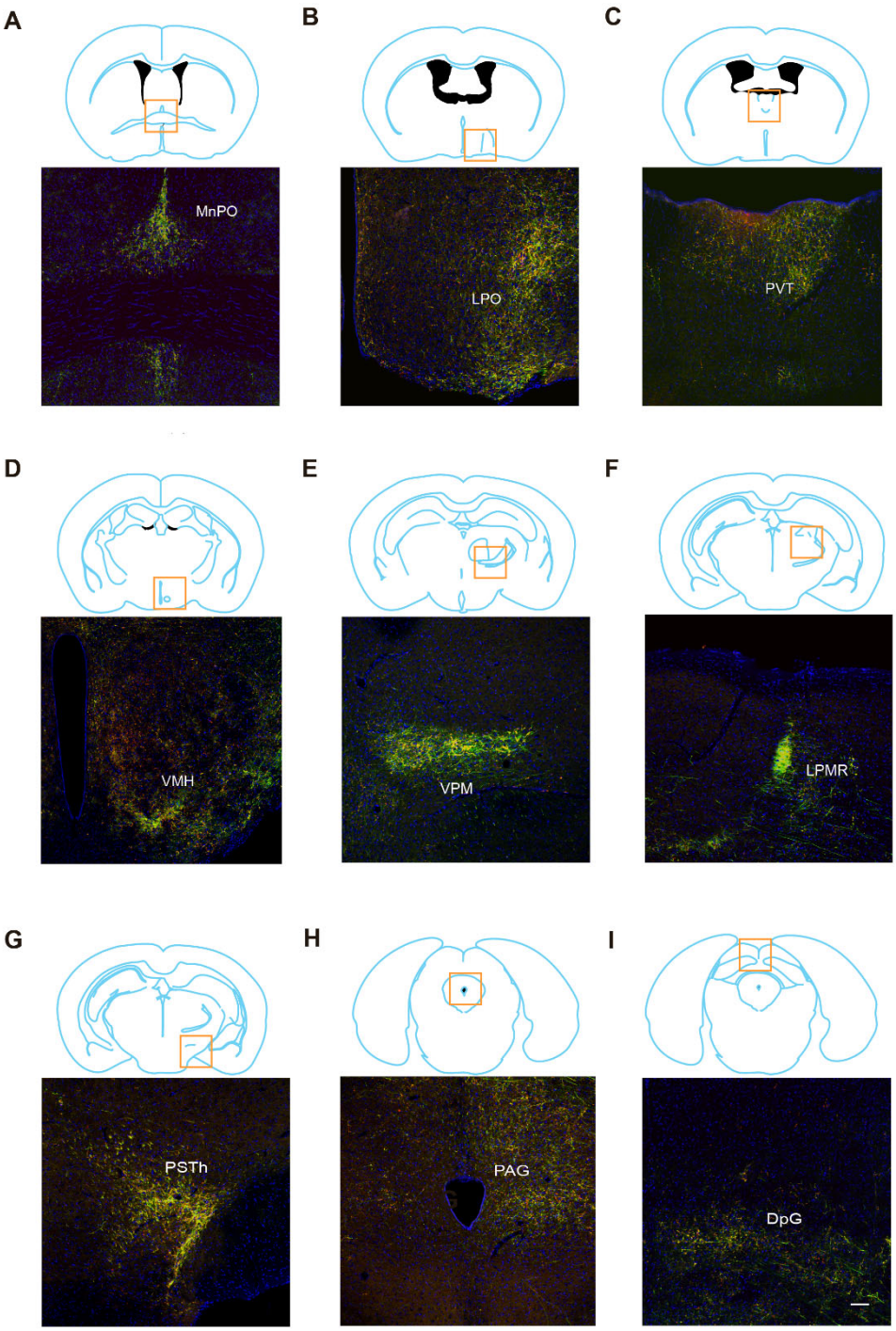


1293

1294